NATIONAL ADVISORY COMMITTEE FOR AERONAUTICS

TECHNICAL MEMORANDUM 1253

FLOW MEASUREMENT BY MEANS OF LIGHT INTERFERENCE

By Th. Zobel

Translation of ZWB Forschungsbericht Nr. 1167, February 1, 1940

Washington
August 1949

NATIONAL ADVISORY COMMITTEE FOR AERONAUTICS

TECHNICAL MEMORANDUM 1253

FLOW MEASUREMENT BY MEANS OF LIGHT INTERFERENCE*

By Th. Zobel

Abstract: There has been under development for the high-speed wind tunnel of the LFA an optical measuring arrangement for the qualitative and quantitative investigation of flow. By the use of interference measurements, the determination of density at the surface of the bodies being tested in the air stream and in the vicinity of these bodies can be undertaken.

The results obtained so far in the simple preliminary investigations show that it is possible, even at a low Reynolds number, to obtain the density field in the neighborhood of a test body by optical means. Simple analytical expressions give the relation between density, pressure, velocity, and temperature.

In addition to this, the interference measurement furnishes valuable data on the state of the boundary layer, that is, the sort of boundary layer (whether laminar or turbulent), as well as the temperature and velocity distribution.

Contents:

*"Strömungsmessung durch Lichtinterferenz." Zentrale für wissenschaftliches Berichtswesen über Luftfahrtforschung (ZWB) Berlin-Adlershof, Forschungsbericht Nr. 1167, February 1, 1940.

I. INTRODUCTION

The development of an optical measuring technique for the investigations in the high-speed wind tunnel of the Herman Göring Aeronautical Research Institute at Brauschweig (fig. 1) rests on the basic idea that fundamentally, the introduction of any mechanical measuring device in the high-velocity flow must be avoided if the results of the measurement are to be free of interference effects. An additional point in favor of light as a means of measurement is its unusually high velocity of propagation, as a consequence of which, the most rapid phenomena in the flow can be recorded without any lag at all.

The choice was made of an interference method, with a special separation of the interfering rays, or the Mach-Zehnder principle for the determination of the density field in the vicinity of a body immersed in the flow, and for the additional purpose of determining the pressure distribution on the body being investigated.

The measuring apparatus is arranged for simultaneous observation of the flow pattern with a Schlieren optical apparatus.

II. THE INTERFERENCE AND SCHLIEREN APPARATUS OF THE LFA

The physical principles of the interference method have already been described in other places (references 1 to 5). The basic diagram of figure 2 will aid in understanding the optical measuring arrangement which will be described in the following:

The light from a light source L travels down two equally long but different paths to the image screen B. The two plane parallel glass plates, P_1 and P_2, are made semitransmitting by the evaporation of a thin metal coating, the plane mirrors S_1 and S_2 are completely reflecting. The light impinging on plate P_1 is divided into two equally bright portions, one of which is reflected and the other is transmitted through the plate.

The two portions of the beam go from plate P_1 by means of S_1 and S_2 to the plate P_2 and can then be made to interfere.

A presupposed condition requirement for obtaining the interference pattern is a careful initial adjustment of the device, in which all the mirrors and plates are parallel and the two light paths must be exactly equal. The rays then interfere at infinity.

In order to bring them into interference on a previously chosen image plane, there must be a certain angular displacement between P_1 and P_2, so that the two portions of the beam pass through the image plane B (fig. 3). There then originates in this plane a streak or fringe system that can be changed at will with respect to the direction and breadth of the streaks by means of a suitable mirror mounting.

If one places in one of the two bundles of rays the so-called measuring ray, a medium under investigation which is of different density from that in the undisturbed air, the formation of the interference fringes results. The magnitude of the distortion of the fringes is a direct measure of the density in the medium under investigation.

The angular displacement in the interference refractometer defines the direction of the fringe movement in the interference image (fig. 3).

If the two interfering rays intersect on the one or the other sides of the central plane of the image area B, the direction of the streak displacement will follow with appropriate sign as the circumstances dictate. Figure 4 shows as an example the spacial density field around a burning candle for various angular settings of the interferometer.

The sensitivity of the interference technique can be varied at will through wide limits by choosing the width of the bands. The measuring technique can be adapted in a satisfactory manner to the immediate problem under investigation by choosing the arrangement of the streaks and the sign of the streaks' distortion.

If one is concerned with the investigation of bodies immersed in the flow as is required in aerodynamic applications, then one can determine by choice of the fringe width, the pressure distribution at very many test points on research bodies without having to make pressure orifices in the test object.

In addition to this, there can be obtained from the density field, determined by the interference method, data on the potential flow in the neighborhood of the test body, as well as valuable information on the condition of the boundary layer.

The Schlieren technique is used to obtain simultaneous qualitative observations of the flow conditions (fig. 2). Light of another wave length from a source L' is directed by a partially transparent plane parallel plate P' over the measuring arm of the interferometer and traverses the test medium in the same direction and at the same time. Following this, the Schlieren rays are let out of the

interferometer beam by the second partially transparent plate P'' and passing through the Schlieren diaphragm also fall on the image screen B. A Schlieren image of the flow condition is formed there with the same scale as the original.

Figure 5 shows the completed interference Schlieren apparatus of the LFA with a schematic representation of the ray paths. The light L of a high-pressure mercury lamp (above) of the greatest possible light intensity goes from a small mirror 1 to a concave mirror 2, goes from there as parallel light to the mirror 3, which redirects it, and then traverses the four plate system as shown in figure 2. After the two interfering portions of the ray are again united at plate P_2, the light path continues over mirrors 4 and 5 to the concave mirror 6 of long focal length (f = 3.5m), which produces an air image of the test area G in the wind tunnel after passing over the additional mirrors 7, 8, and 9. Mirror 9 is partially transparent, so that the light hitting it is split into two parts, of these the more intense portion goes to the air image, and the weaker light is directed by mirror 10 to a ground glass for observation. A color filter inserted in the path of the beam provides for the selection of the wavelength λ_1 = 5770-5790 AU which is especially adapted to our needs.

The variation of the optical path in the measuring beam of the interferometer caused by the index of refraction of the glass in the wind tunnel and at the end plates of the model is equalized by a compensator in the second arm.

The light path for the Schlieren apparatus starts at the light source L' (below) and goes from mirrors 11 and 12 to the concave mirror 13. From there the parallel beam goes to the semitransparent plate 14 in the measuring arm of the interferometer and, along with it, goes through the glass windows in the walls of the wind tunnel and the end plates of the model being tested and through the air stream (fig. 2).

The plate 15 again deviates the Schlieren beam and the beam is redirected by the mirror 16 to the concave mirror 17. This makes on its part with equal focal length and object distance, that is, also with the same image scale, an image of the test object in the plane of the air image, as well as on the ground glass. The path, after passing the Schlieren shutter, is by way of mirrors 18 and 19.

With this apparatus the variations during the test can be continuously observed in a soundproofed test cell by both optical apparatus, while the same events may be independently photographed or filmed. A high-speed motion-picture apparatus makes it possible to take successive exposures with a large number of frames per second

of particularly interesting and rapid events, while the light source can be controlled by the motion-picture camera to run in a heavily overloaded condition for a short time (and therefore increase the light intensity).

For special investigations of short-period events, there is also provided as an additional light source a spark generating arrangement, which permits of single exposures with discharge times of about 10^{-6} seconds (fig. 5). It can be seen at the left of the diagram that, by simple repositioning the two mirrors 1 and 11, the light of the spark passes down the two previously described light paths of the optical arrangement. The optical arrangement of figure 5 was chosen to provide the long paths to the photographic image in the device itself and to enable photographic exposures as well as observations to be made near the measuring location.

All the optical mechanical parts are combined in a large measuring carriage, which is built as a box carriage, that can be isolated from the surroundings by heat absorbing means, in order to keep temperature disturbances from the neighborhood of the measuring device.

All the mirrors and plates are fully cardon mounted, and can therefore be shifted in angle about two axes at right angles to one another. After the adjustment of the device has been completed, most of the mountings are clamped. Only plates P_1 and P_2 of the interferometer, as well as the compensator and the two plane parallel plates 14 and 15 of the Schlieren system, may possibly have to be moved during the operation of the equipment.

The drives for the mirror mountings as well as the optical components[1] themselves must be of the highest precision, as displacements of the mirrors to fractions of a second of arc must be possible.

The adjustable mirror assemblies are fitted with multiple worm-gear drives for fine control. The step down is about 1 to 73,000,000. The mirrors can be operated electrically by remote control from within the test room, and with this control one can obtain as the minimum angular displacement about 1/10 second of arc. In addition, there is provided an electrical repeater for the angular setting from the drive mechanism itself, so that there is available at the measuring desk an accurate survey of the adjustment of the optical test equipment.

---

[1]All optical components were produced by the firm of Halle Nachfolger, Berlin-Steglitz. The excellent full cardon mirror mountings for the interferometer were also manufactured by the Halle company from our design proposals.

The frame of the measuring equipment itself is based on principles derived from vibration technology, that is, it is connected to the external movable supporting framework with accurately graduated sets of springs. In this manner, all vibrations from the surroundings from the wind tunnel and from the building are isolated from the measuring apparatus.

III. INTERFERENCE MEASUREMENTS

During the time to the present, while the framework is being completed, the interferometer portion of the equipment has been in use for about half a year with a provisional frame unit of the original size. The first investigations of the optical beam compensation, as well as the angular sensitivity of glass plates, which are inserted in the path of the measuring beam as boundary windows for the wind tunnel and the model, have already been completed. A small test tunnel has also been built, so that it is possible already to make flow measurements by means of light interference.

The bulging of the interference fringes as compared to the undisturbed fringe field (without air flow) is a direct measure of the density from the relation:

$$\Delta\zeta = \frac{b \times L \times (n_\infty - 1)}{\lambda \times \rho_\infty} \times \Delta\rho$$

Wherein the symbols are as follows:

$\Delta\zeta$(mm) fringe bulging

b(mm) distance between two undisturbed interference fringes

$n_\infty - 1$ index of refraction of undisturbed medium = $0.000293 \times \frac{273}{T_\infty}$

ρ_∞ $\frac{kg \times s^2}{m^4}$ air density in undisturbed region

λ(mm) wavelength of light used (5790 AV)

L(mm) length of path which light traverses in medium of altered density

The magnitude $\frac{\Delta\zeta}{b}$ is one which is independent of the scale size of the image and which can be determined from every fringe photograph.

In an adiabatic change of state, the relation between the density and the static pressure in the flow field is given by the equation:

$$\frac{p_1}{p_2} = \left(\frac{\rho_1}{\rho_2}\right)^K$$

If the static pressure on the surface of a body in the flow is to be determined, then designate p and ρ as pressure and density at the test body, p_∞ and ρ_∞ pressure and density in the free stream. There then follows as a first approximation:

$$\frac{p - p_\infty}{p_\infty} = K\frac{\rho - \rho_\infty}{\rho_\infty}$$

At a Mach number greater than $M = 0.5$, the exact formula for the adiabatic

$$\frac{p}{p_\infty} = \left(\frac{\rho}{\rho_\infty}\right)^K$$

should be used.

For the pressure coefficient $\frac{\Delta p}{q}$ commonly used in pressure-distribution measurements one then gets (for $M = 0.5$) the following expression:

$$\frac{\Delta p}{q} = \frac{p - p_\infty}{q_\infty} = K \times \frac{p_\infty}{q_\infty} \times \Delta\rho$$

But the quantity $\Delta\rho$ is known from the optical measurement. Consequently we have:

$$\frac{\Delta p}{q} = K \times \frac{p_\infty}{q_\infty} \times \frac{\lambda}{L(n_\infty - 1)} \times \frac{\Delta\zeta}{b}$$

Numerical Example

For evaluating a density field: Span $L = 170\text{mm}$

Fringe spacing from the photograph $b = 2.7\text{mm}$. Impact pressure in the test section $q = 350\text{kg} \times \text{m}^{-2}$, $p = 9975\text{kg} \times \text{m}^{-2}$ at a temperature of 18° C.

$$\frac{\Delta p}{q} = 1.4 \times \frac{9975}{350} \times \frac{5790 \times 10^{-7} \times 291}{170 \times 0.000293 \times 273} \times \frac{\Delta \zeta}{b}$$

$$\frac{\Delta p}{q} = 0.495 \frac{\Delta \zeta}{b} = 0.183 \, \Delta \zeta$$

For a given fringe spacing it is, therefore, only necessary to multiply the fringe shift by a constant factor to obtain the pressure coefficient.

It is apparent from the final equation for Δy, that the measuring technique must be extraordinarily sensitive to the smallest change in density since the measured fringe shift in the interference pattern is directly proportional to the fringe spacing as well as the length L (with airfoils, L is the span). The great sensitivity results from the fact that the variations in density existing at each point in the flow field are integrated over the entire extent of the test object (L). By choosing these two values, b and L, one can accommodate the sensitivity of the technique within wide limits to the research problems of interest at the moment.

It is mentioned, in this connection, that the theory of potential flow considers air as an incompressible medium up to a stream velocity of 100 meters per second, that is, it is assumed that the density remains constant in this flow region. The fact, however, that in reality there is a density variation associated with every velocity variation, forms directly the basis of measurement for the interference technique. The assumption that the density is constant in potential flow for each plane section of the field of flow produces a negligibly small error. The value of the integral of this small quantity taken over the length L gives, however, a displacement of the interference fringes which is sufficient for measuring purposes.

The assumption existed at the beginning of the development of this optical technique for flow measurements, that in any event an attempt to further increase the sensitivity of the method will be required. The results obtained to date have already shown, however, that with a small model (170mm span) and with a normal stream velocity sufficient fringe shift will be obtained. With this, the conditions of the problem have been fundamentally altered.

If it is realized that the magnitude of the fringe distortion is not only proportional to b and L, but also to the density variation $\Delta \rho$ and therefore at low speeds to the square of the speed and in compressible flow to about the velocity itself, then large fringe shifts should result in the investigations in the high-speed wind tunnel. If the span is 10 times and the stream velocity 4 times

as great as that in the preliminary investigations presented, then the expected fringe shift with the previously used fringe spacing should be 40 times as great. It then may be possible, the necessary circumstances permitting, by utilizing the highest possible stream velocity in the high-speed wind tunnel to substantially decrease the span of the model as well as the fringe spacing in the interference image. By terminating the model with end plates (plane case) no aerodynamic difficulties are introduced. The choice of the very narrow interference fringes only increases the number of test points on the body being tested. There can then be used in the evaluation, as one pleases, the measuring points which are believed to be important.

Figure 7 shows the density field of a cylinder of length L = 170 millimeters and diameter D = 25 millimeters in flow at a velocity of 75 meters per second, with both of the possible signs of fringe shift available by adjusting the angles in the interferometer. It is obvious that in the examples given, the direction of the shift in figure 7(a) is more advantageous for evaluation as many more measuring points are available in the vicinity of the stagnation point and in the region of increased velocity. The marked change in density from potential flow to the stagnant region may be noted, as well as the uniform mean value of the density behind the drag-producing body. A very intense energy loss, which should also be noted, takes place in the two vortex trails at a distance behind the test object of about one-body diameter, this loss being a result of rapid velocity fluctuations. The fuzziness of the interference field is a result of the fact that the density fluctuation occurs more rapidly than exposure time of 1/200 second which was used. The velocity with which the density variation takes place can be found from the picture sequences in a slow motion picture.

Figure 8 shows the pressure distribution on the circular cylinder over the angular range of 0° to 180° as evaluated from the interference measurements. A pressure distribution from R & M 1210 is drawn on the same graph for comparison. The comparison shows that the optical measurements give a reading with the proper trend, and that usable absolute values may be obtained from the fairly primitive arrangements of the small test tunnel. The wind tunnel does not as yet have any screen and, therefore, a very poor velocity distribution results in the test section. The tunnel probably also has a very high degree of turbulence.

Figures 9 and 10 show the density field of elliptical cylinder of axis ratio of 4 to 1 for the two different angles of attack of 0° and 8° and with both signs of fringe displacement. Figures 11 and 12 show the results of the interferometer measurements for both angles of attack and, for comparison, the result of the calculation of the pressure distribution for zero angle of attack.

It should be noted, as shown by the results of the measurments in NACA Rep. 652, that the pressure distribution of an elliptical cylinder is quite dependent on the Reynolds number and the amount of turbulence in the tunnel. The shape of the pressure-distribution curve obtained by interferometer is very similar to that presented in the NACA report as the result for a body of different axis ratio. Agreement of the absolute values with the measurements of other tunnels and with the theory can not be expected for the reasons stated.

In addition, investigations were made of airfoil sections. Figure 13 shows a series of angles of attack for the Göttingen 387 section which were taken for the pressure-distribution measurements. As the section in question has a thickness which approaches 10 percent of the diameter of the tunnel, induced flow effects introduce appreciable changes in the flow field at different angles of attack. Therefore, only $\alpha = 0^\circ$ and $\alpha = 5.7^\circ$ may be evaluated and compared. The velocity in the test section cannot be determined for other angles of attack. The records are presented for the purpose of studying with them the evaluation of the fringe shift with unfavorable signs. The fringe shift in the region around the nose and near the stagnation point should be observed.

Figure 14 shows the comparison of results of the Göttingen pressure-distribution measurements with those of the interferometer for the Göttingen 387 section at $\alpha = 0^\circ$. The deviation in the pressure curve on the pressure side of the airfoil is a result of the distortion caused by the support.

Figures 15 and 16 show the effect of the support for an angle of attack $\alpha = 5.7^\circ$ for attachment on either the pressure or suction side of the wing. Figure 17 presents the pressure distribution of the undisturbed wing (without support) in comparison with the Göttingen measurements of pressure distribution.

In the case considered the disturbance caused by the support is very noticeable, but this disturbance can be confined to the immediate vicinity of the wall and the span of the model is also quite small. In the high-speed wind tunnel the proportions are much more favorable. In addition, there is no problem in constructing the model so that the support is located outside of the end plates and so is completely prevented from disturbing the flow on the wing itself.

Figures 18 and 19 show the flow on a 10-percent-thick Joukowsky section for a series of angles of attack up to the separation of the flow.

From the large group of interferometer records it can be noted that distortions which can be evaluated are produced in the fringes,

in the stagnant region immediately behind a drag-producing body, and also at the greater distances from the model in the wake. At the present time a method of evaluation for drag determination[2] is being worked out.

Up to this point it has been tacitly assumed that the interference fringes were a result of the use of monochromatic light, which completely filled the image field with interference fringes. There was used also, in the previously presented example, continuous homogeneous light. There are, however, applications where the identification of individual fringes arises. For this reason, it is necessary to particularly single out certain fringes. This can be done by the so-called null interference, in which the individual fringes show up with different strengths and sharpness. If light containing several wavelengths is used, then the resulting interference fringes will have different widths corresponding to the appropriate wavelengths. The result of this is a building up of groups of fringes. The light is completely cut off at the point between the individual groups of fringes where the maximum intensity of the system due to one color coincides with the minimum of that of another, and no interference fringes appear. There is only one group of fringes with a highly dense interference pattern, the so-called null interference, which is formed on the line of symmetry of all the coherent points of light. The existence of this null interference is exactly the criterion for the complete adjustment of the interferometer, in which the two light paths (figs. 2 and 3) must be so exactly of the same size, that they differ from one another by only a fraction of a half wavelength of the light being used.

Figure 20 shows a photograph of the null interference with mercury light. The null interference fringes are identified in a positive manner by comparing their greater intensity with that of the remaining fringes.

Figure 20 also shows how the null interference may be used in a valuable manner, for example, to determine the velocity in a closed tunnel. If the upper portion of the exposure of the interferometer field shows the image for the known outlet condition in the tunnel without flow ($v = 0$), there the lower portion of the exposure shows the fringe field displacement with air flow. The shift is a direct measurement of the variation in density and therefore of the flow velocity. In a similar fashion, temperature and fluid flow distributions and the like, in which the medium being tested at the time remains homogeneous but changes density, may be measured.

---

[2]A report especially on the evaluation techniques for the interferometer will be published.

IV. BOUNDARY LAYER INVESTIGATIONS

The interference photos of the flow around airfoils have already indicated very interesting results which were in addition to the pressure-distribution measurements. The growth of the boundary layer on the surface of the section can be already seen as can its increase in thickness in the direction of the section chord. The examples presented up to now have been excluding the turbulent boundary layer, which increases to no more than a few millimeters at the edge of the airfoil.

The laws of potential flow apply only beyond the limits of the boundary layer. The measuring points for the interference evaluation are therefore on the edge of the section after a change in direction at the boundary. At locations where no boundary layer is present, the test points lie on the surface of the section.

Since Bernoulli's equation does not apply within the boundary layer, but as the static pressure must be constant throughout the entire thickness of the boundary layer in the direction perpendicular to the surface, the fringe shift in the interference image results purely from a temperature effect in the friction layer. At the point of greatest heating, which is the point on the surface of the section where the velocity value is zero, the fringe shift is the greatest. The variation in temperature in the boundary layer itself may be determined from the general equation of state $\frac{p}{\rho} = R \times T$, since the state's pressure at the edge of the boundary layer is known from the pressure in the potential flow.

The question of whether the assumption of constant pressure in the boundary layer is justified can be answered with the aid of the interference records. If a pressure variation did exist within the boundary layer, then this variation should be noticeable in an additional shift of the fringes. The extension of each interference fringe in the potential flow until it reached the surface of the section should lead to points which would show a sidewise shift of the fringes from the points on the edge of the boundary layer. This amount would then indicate the variation of the static pressure in the boundary layer. However, it is clearly seen in all the interferometer records that at the locations where the boundary layer is thick, the fringes run close to the vertical, and in other locations where they are bent, the boundary layer is entirely or nearly zero. But in no case has a fringe shift been established which was not negligibly small.

Previously there was, in general, no method of measurement which enabled one to make the boundary layer visible and to make measurements

therein as does the interference method. Figure 21 presents the data on the boundary-layer thickness which exists on a Joukowsky section at the three angles of attack 0°, 4°, and 8°. (Compare fig. 18.) The measured boundary-layer thickness for a somewhat thicker symmetrical Joukowsky section at 0° from R & M 1315 is introduced for comparison. Figure 22 shows the boundary-layer thickness for an elliptical cylinder for 3 different angles of attack. (Compare also figs. 9 and 10.)

An important case in the study of the boundary layer is given by the flat plate aligned with the flow. Since the pressure on its surface is that of the undisturbed stream and nevertheless a marked density variation exists, this would indicate an effect entirely ascribable to temperature.

Figure 23 shows the density field for a flat plate for two different fringe widths and enlargements of portions of the field to show the density effects in the boundary layer for a Reynolds number of 800,000.

Exact investigations of conditions in the boundary layer, under which the transition from laminar to turbulent boundary layer takes place will be initially undertaken with the less objectionable aerodynamic arrangements of the high-speed wind tunnel with information on the degree of turbulence of the tunnel. A means will then be available on account of the large span of the model of making the laminar boundary layer also visible at small velocities.

V. ANALYTICAL RELATIONS BETWEEN DENSITY, PRESSURE, VELOCITY, AND TEMPERATURE

Symbols:

p	pressure	at a chosen point of flow field
ρ	density	
T	absolute temperature	
v	velocity	
p_∞, ρ_∞, T_∞, v_∞	corresponding values in undisturbed flow at a great distance from body	
p_s, ρ_s, T_s, v_s	corresponding values at outer edge of boundary layer	

Δp	$p - p_\infty$
$\Delta\rho_1$	$\rho - \rho_\infty$ (in potential flow)
$\Delta\rho_2$	$\rho - \rho_s$ (in boundary layer)
$K = \frac{c_p}{c_v}$	1.4 for air
$M = \left(\frac{V}{a}\right)$	Mach number in undisturbed flow
a	velocity of sound in undisturbed flow

Professor Schlichting[3] has arrived at the following simple equations by an analytical attack on the relations between density, pressure, velocity, and temperature based on the general equation of state and the law of conservation of energy:

1. For Potential Flow

(a) At low Mach numbers.- Relation between pressure and density:

$$\frac{p - p_\infty}{p_\infty} = K \times \frac{\rho - \rho_\infty}{\rho_\infty}$$

Relation between temperature and density:

$$\frac{T - T_\infty}{T_\infty} = (K - 1)\frac{\rho - \rho_\infty}{\rho_\infty}$$

Relation between velocity and density:

$$\frac{v^2 - v_\infty^2}{v_\infty^2} = -\frac{2}{M_\infty^2} \times \frac{\rho - \rho_\infty}{\rho_\infty}$$

(b) At high Mach numbers.- Relation between pressure and density:

$$\frac{p}{p_\infty} = \left(\frac{\rho}{\rho_\infty}\right)^K$$

[3]Professor Schlichting is publishing a special report on the theoretical work.

Relation between temperature and density:

$$\frac{T}{T_\infty} = \left(\frac{\rho}{\rho_\infty}\right)^{K-1}$$

Relation between velocity and density:

$$\frac{v^2 - v_\infty^2}{v_\infty^2} = \frac{2}{(K-1)M_\infty^2}\left[1 - \left(\frac{\rho}{\rho_\infty}\right)^{K-1}\right]$$

Frictionless flow in which no energy exchange takes place with the surroundings by conduction, radiation, or convection is assumed in developing the calculation.

2. For the Boundary Layer

Relation between pressure and density:

$$p - p_s = 0$$

Relation between temperature and density:

$$\frac{T - T_s}{T_s} = \frac{\rho_s - \rho}{\rho} = \frac{-\frac{\rho - \rho_s}{\rho_s}}{1 + \frac{\rho - \rho_s}{\rho_s}}$$

Relation between velocity and density:

$$\frac{v^2 - v_s^2}{v_s^2} = \frac{-2}{(K-1)M_s^2}\frac{\rho_s - \rho}{\rho} = \frac{2}{(K-1)M_s^2}\frac{\frac{\rho - \rho_s}{\rho_s}}{1 + \frac{\rho - \rho_s}{\rho_s}}$$

In this case, as compared to the analytical development for potential flow, the assumption of conservation of mechanical energy (Bernouilli's equation) is not made, but there is merely substituted for it the usual hypotheses of boundary-layer theory that the pressure in the boundary layer is constant along a perpendicular to the surface.

As the equation for the relation between the density and the temperature in the boundary layer neglects a heat transfer, the

calculated temperature distribution in the boundary layer will give values which are too high.

An evaluation of the interference photographs was undertaken for the flat plate example (fig. 23).

Figure 24 shows the calculated velocity distribution in the boundary layer of the flat plate for the substitution of the 1/7 power in the theoretical relation and gives for comparison the results of the interference measurements.

Figure 25 gives the calculated temperature distribution in the boundary layer of the flat plate and the temperature distribution resulting from the interference measurements. It can be seen that the interference measurements, which are a direct expression of the existing density, give lower values of temperature than those which are calculated. This result was to be expected, as the calculations neglect any lowering of the temperature in the boundary layer by conduction, radiation, and convection. Whether the difference of the two results gives an accurate absolute value for the decrease in temperature resulting from heat loss will have to be shown by exact investigations in the high-speed wind tunnel.

VI. OTHER POSSIBLE APPLICATIONS OF THE INTERFERENCE METHOD

The fact that the optical measurements can be adapted in a completely inertia-free manner to very rapidly changing conditions of movement (fig. 26) gives entirely new and not yet perceived possibilities for the application of the interference technique. There are of interest in this connection in particular those unstationary conditions on wings, in which in certain circumstances the train of events occurs faster than the flow can follow. The simplest example of this sort is the unsteady growth of lift on the wing accompanying a sudden increase of the angle of attack. Test results, which give a summary of the increase of maximum lift for sudden increases in the angle of attack (Böen effect), do not suffice to clarify the causes of this effect. These measurements also do not give any information on the lift relationship for sudden changes of the angle of attack in the lower range of values for C_L, on the location of the center of lift and on the role of the boundary layer on the unsteady flow condition.

In addition, a very important and complicated problem is offered by the case of the oscillating wing by itself, as well

as those of the wing with fixed extended flap and with free rudder.

Before this there were no methods of measurement which could be used to measure the pressure distribution simultaneously at many points on an oscillating airfoil during its movement and which would, in addition to this, also give data on the conditions in the boundary layer.

It is even difficult to establish very many pressure measuring points on a normal small airfoil model for static investigations at high speed and to lead the bundle of tubes out of the air stream out to the pressure recorder with the least possible disturbance of the flow conditions. The accomplishment of unsteady pressure measurements on an oscillating wing is, however, far more difficult.

The investigation of such problems poses no problem to the interference method, as every instantaneous photograph gives the complete pressure distribution on the section and in the vicinity, as well as the status of the boundary layer.

Previously conducted investigations on an oscillating wing, carried out with the wings oscillating movement in the air stream set at 40 oscillations per second, show, in a slow-motion film, changes in the density field with every movement of the airfoil. Each individual interference photograph contains all the necessary test data for the examination and evaluation of the conditions of flow. Because of this we are presented with the possiblity of ascertaining on the oscillating wing the relations existing with regard to the rudder setting as well as the transmission of pressure waves on the airfoil surface at high velocities and the variation in lift and the center of pressure which depend on these.

Figure 27 shows some fringe photographs from a slow-motion film (see the original fig. 27(a)) of a Joukowsky wing oscillating at $n = 40$ cycles per second in an air stream with a velocity of 75 meters per second.

It should be very desirable to apply the interference technique to the investigation of radiator shapes for high flight velocities. It is known that the resistance characteristics of axial radiators with outlets on the fuselage are quite favorable when the cooling air flow exists on the fuselage with a speed greater than that existing at the outer location and then travels along the remainder of the body. Until now, there have been only conjectures about the reasons for such effects appearing in an unheated radiator. Even pressure-distribution measurements, which can be carried out for many test

points only with great expense, do not clarify these questions sufficiently, if the conditions existing in the boundary layer are completely disregarded.

With a plane radiator model the interference measurements give the over-all density relations, that is, the pressure and velocity, on the external body, as well as at each point in the ducting and the diffuser and, in addition to these, data on the boundary layer and of the influence thereon of the cooling air flow. The development of a suitable nose shape at the entrance of the radiator for different size of ducting and angles of attack can also be undertaken by interference measurements in a similar manner. If the conditions existing in the plane problem are known, it is then possible to connect the results to the axially symmetrical case.

If the results of the plane problem are connected to the case of an axially symmetrical body developed into a plane, one will certainly approach very much closer to the time conditions than by a flow investigation of the spatial density field (at zero angle of attack for each case). Because of the fact that the light rays pass through different zones of differing and unknown density in the spacial density field, a certain uncertainty always remains in the interpretation in particular. The investigation of spacial density fields is an important question of the immediate future.

The use of the representation of the problem by the plate case has the great advantage of the unequivocalness of the conditions and the evaluation, while in the present state of development we must be content with a fairly inconvenient graphical interpolation method as a means of approximation. There is, in addition, a great advantage of the plane problem, in that the interference measurements also guarantee an insight to the conditions within a body, as for example, the diffuser and flow passages of radiators, in crevices and behind interfering projections in models and the like.

In this way a number of possible applications of the interference technique can be made to problems, which could not be undertaken with previous methods of measurement.

Figures 28 to 31 show as an example an NACA radiator cowl as a plane model in an air stream of 75 meters per second velocity in two different configurations, one with a somewhat extended thoroughly rounded hub and one with a short normal (NACA) slightly rounded hub. In figures 28 and 30 the air passage is open, in figures 29 and 31 it is closed by a plug. Figure (a) shows the unaffected interference fringe field without the air stream; figures (b), (c), and (d) show the conditions of flow for three different angles of attack 0°, 4°, and 8°.

The interference fringe photographs give information on the flow conditions in and on the radiator cowl and on differences in the characteristics of the various cowl shapes even before a numerical evaluation is undertaken. With the simple relations given on pages 9 and 10 the interference fringe photographs can be read to obtain the velocity appropriate to each point on the hub or in the air duct. Reference will be made here only to certain differences which are readily observed in examining the radiator configurations. Increased inflow velocities can be recognized in the region of the nose from the sharp bends in the interference fringes and their changes with angle of attack. The hub and radiator cowl operate in the closed duct case of figure 29 as an ordinary section to which the flow conforms. The expression follows clearly that as the stagnation builds up in the obstructed air passage, the flow around the external body will take place as if around a regular section.

Figures 28(b), 28(c), and 28(d) show that the increased velocity on the extended hub is appreciably greater than that on the blocked passage configuration. It can be recognized from this that the two noses of the hub and of the radiator cowl set up their own independent flow profiles when flow takes place in the duct. The duct velocity seems to be greatest at $\alpha = 4^\circ$, while at $\alpha = 8^\circ$ a shift in the location of the stagnation point has already taken place. At 8° the flow has not yet separated at the nose of the cowl.

In figures 28(b) and 28(c) a distinct jump in density may be recognized on the suction side of the cowl behind the region of the maximum increase in velocity, which probably represents the transition from the laminar to the turbulent boundary layer. The portion of the boundary layer lying behind this point can be clearly interpreted as turbulent just from its great thickness. The laminar-turbulent transition point moves further forward at the higher angles of attack. The smooth portion of the radiator cowl is similar to a flat plate. (Compare fig. 23.)

Figures 30 and 31 show that the flow is already separated at 0° angle of attack with the nose that is only slightly rounded. The difference between the case with increased velocity over the outer body and that with zero velocity in the blocked air passage may be clearly recognized from the series of photographs of figures 31(b), 31(c), and 31(d). The flow through the radiator with short hub affects the external flow in an appreciably stronger and unsatisfactory manner than is the case for the configuration of figure 28. A sharp increase in the thickness of the boundary layer and the approach to the critical condition, where the flow will separate from the external portion of the body, is already noticeable at $\alpha = 4^\circ$. Figure 30(d) shows how the flow on the suction side of the outer portion of the cowl has already separated at $\alpha = 8^\circ$.

It would probably be possible to obtain the desirable condition of no separation if the short hub was rounded off in better fashion and was extended forward a negligibly small amount. In this case the flow through the duct would be opposed by the adverse peak pressure displacement of the long hub at the higher angles of attack. It still remains to be shown whether or not the flow in the last-named configuration remains on the body at the high angles of attack.

As an additional example in figures 32 to 35 there are shown some interference photographs of flow in a jet-type radiator with a very large air passage. In figures 32 and 33 the air passage has a built-in flow drag plate with horizontal slits which has a transmission of about 50 percent. Figure 32(a) indicates (compare also fig. 7) how the density is smoothed out to a nearly constant mean value over the whole cross section only a short distance behind the drag plate. (All of the interference fringe fields are entirely free of retouching!)

The velocity of flow at the various points of the air passage can be directly determined from the distortions of the interference fringes. The right-hand vertical series of photographs (figs. 33 and 35) show the arrangement with an extended flap in which an appreciable increase of velocity through the radiator is very clearly seen. Figures 34 and 35 are the photographs of the interference fringes for flows through the open-jet passage with and without the effect of the extended flap.

These examples serve only to show the simple manner in which interference measurements permit one to carry out with a minimum of expense for research apparatus (once an interferometer is available) investigations of this kind and to give a glimpse of the many phenomena still unknown. The quantitative data thereto follow from the interference evaluation.

The application of optical measuring technique becomes more urgent with the increase of flight speeds, while these techniques have the great advantage that they serve to make the conditions measurable and visible without permitting any but the least disturbance to those conditions. By using interference measurements, the additional advantage is attached that all pressure holes and tubing are eliminated on the model and in this way the production of what would otherwise be very complicated and expensive models (compare the models with pressure holes and tubing for high-speed investigations) is very much simplified. It is also a measuring technique of the greatest value as each individual fringe photograph of a slow-motion film made at a high frame frequency contains the record of all the test data of the conditions being tested.

VII. SUMMARY

A new type of optical measuring technique is described for the simultaneous qualitative and quantitative representation of density fields around a body in fluid flow, which has been developed at the LFA Hermann Göring, Braunschweig. The technique has been developed especially for the investigation of compressible flow in the high-speed wind tunnel. The results obtained so far in preliminary investigations with the interference portion of the test apparatus show, however, that it is even possible to obtain at normal velocities density fields around test bodies which are evaluable.

Simple analytical expressions give the relation between the density as determined from the interference and the pressure, velocity, and temperature on the test body and in its vicinity. The method of evaluation used for pressure distribution is explained and the utility of the technique is pointed out by reference to a worked-up example of the interference measurements. At the present time work is underway on the evaluation of interference patterns for drag.

It is also shown that with the optical technique it is possible to make the boundary layer visible for the first time and to obtain quantitative data in the boundary layer. Because of the great velocity of propagation of light, all of the conditions in the flow which occur so rapidly can be recorded in an entirely inertia-free manner by the use of the optical measuring arrangement. Because of the possibility of investigating conditions, which were wholly outside the limits of the previously available techniques, the optical interference measurement is presented with a series of new problems in addition to many more possible applications which at present have not as yet been surveyed.

Translation by Morton J. Stoller
National Advisory Committee
for Aeronautics

VIII. REFERENCES

1. Gehrcke, E.: Die Anwendung der Interferenzen in der Spektroskopie und Metrologie. Braunschweig 1906.

2. Schardin, H.: Theorie und Anwendung des Mach-Zehnderschen Interferenzrefraktometers. Z. Instrumentenkde, Bd. 53 (1933) p. 396, 424 and 430.

3. Dechend, A. v.: Über die genaue Messung der Lichtbrechung in Gasen. Heidelberg 1913.

4. Zobel, Th.: Verwendung von Lichtinterferenzen in der technischen Messung. Z. VDI. Bd. 81 (1937) Nr. 18, p. 503.

5. Zobel, Th.: Entwicklung und Bau eines Interferenzgerätes zur optischen Messung von Dichtefeldern. FB 1008. (Available as NACA TM 1184.)

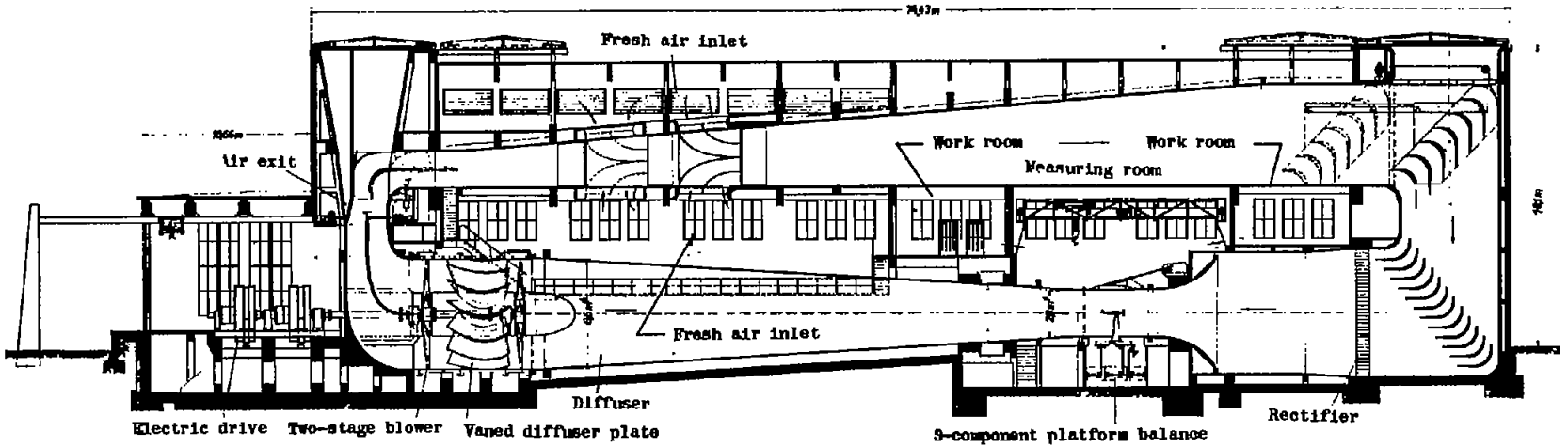

Figure 1.- High-speed wind tunnel of the Hermann Goring Aeronautical Research Institute at Braunschweig.

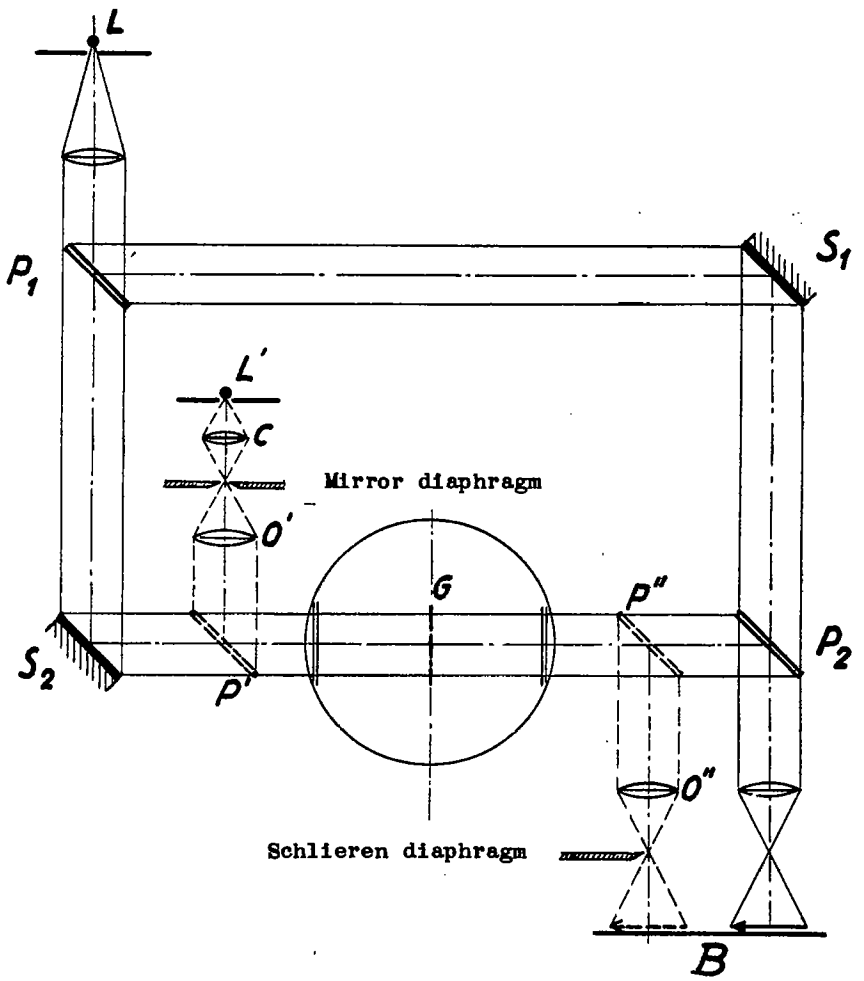

Figure 2.- Basic diagram of the light path in the interference apparatus.

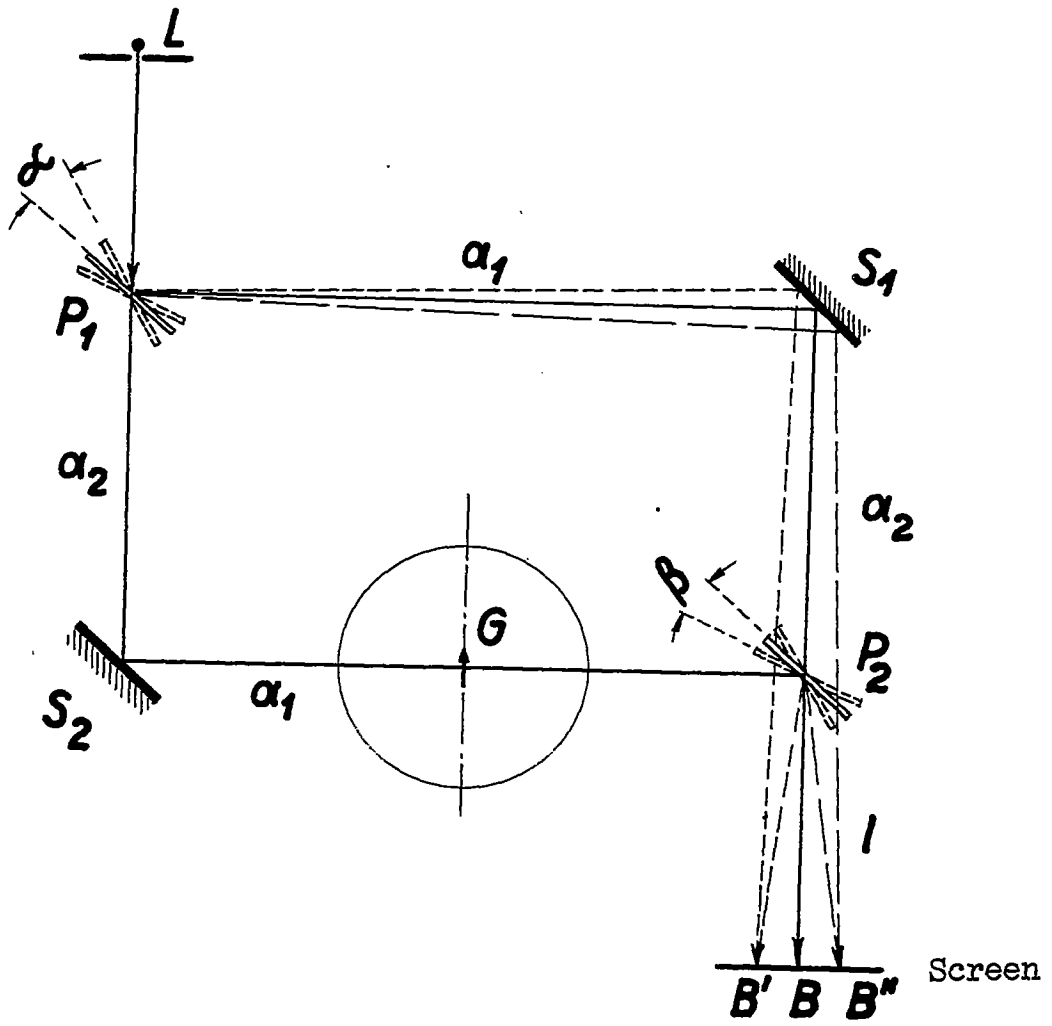

Figure 3.- Angular displacement at the interference apparatus.

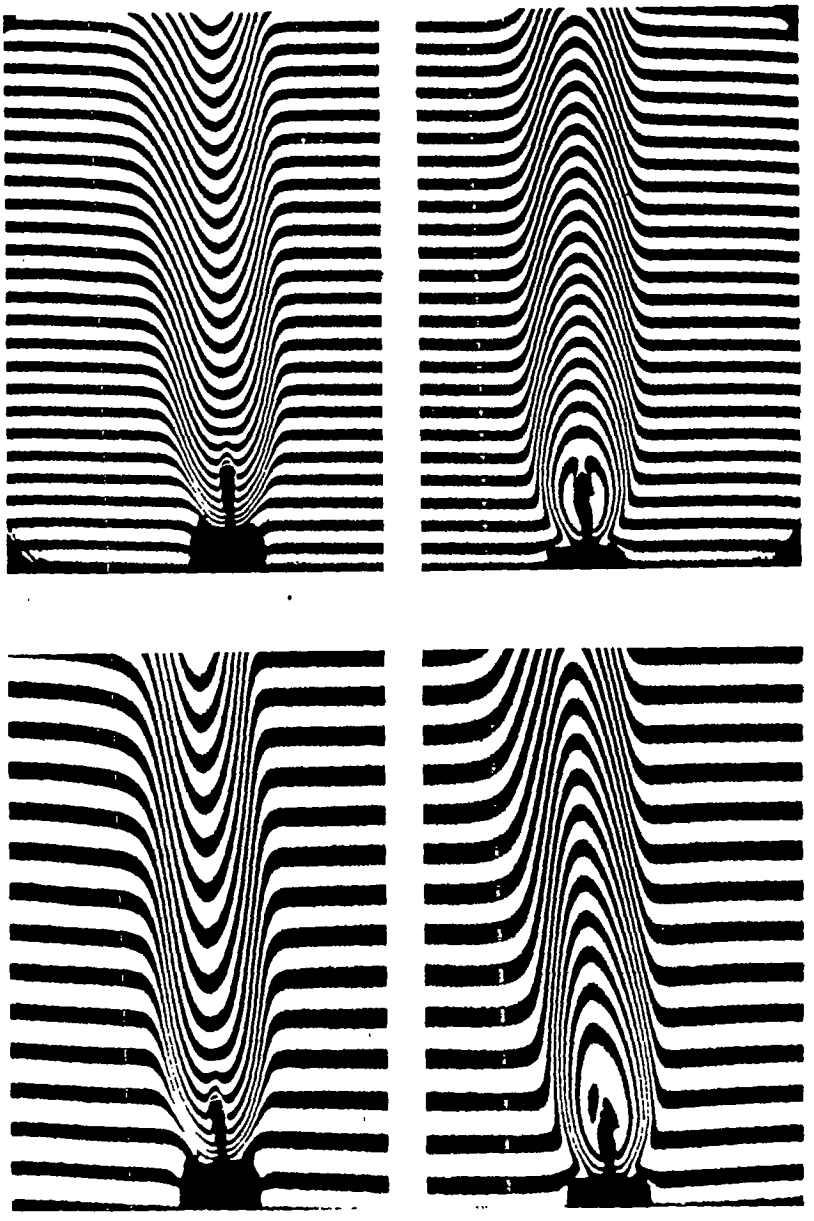

Figure 4.- Spatial density field around a burning flame for two-directional fringe bulging.

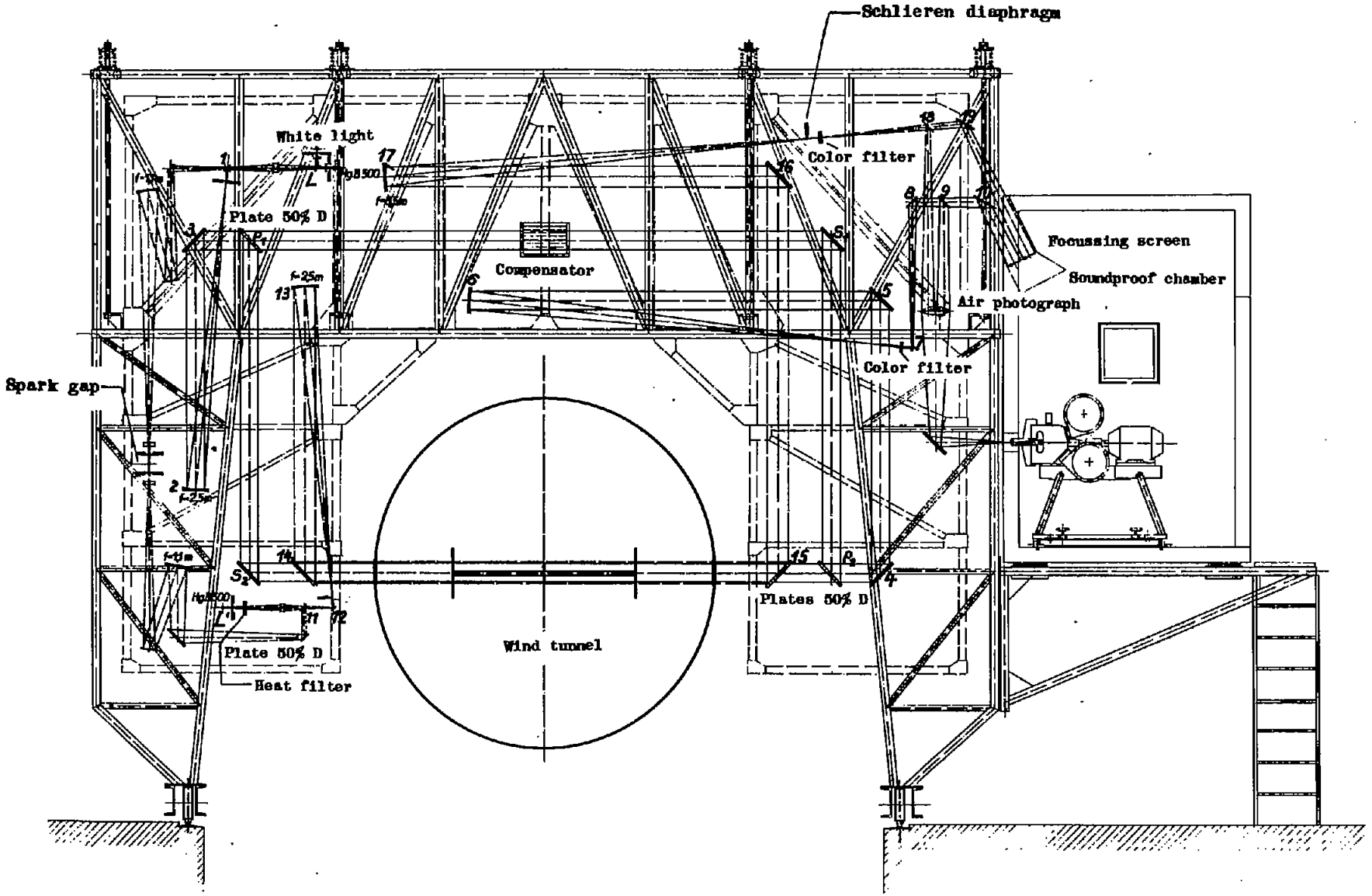

Figure 5.- Interference-schlieren method.

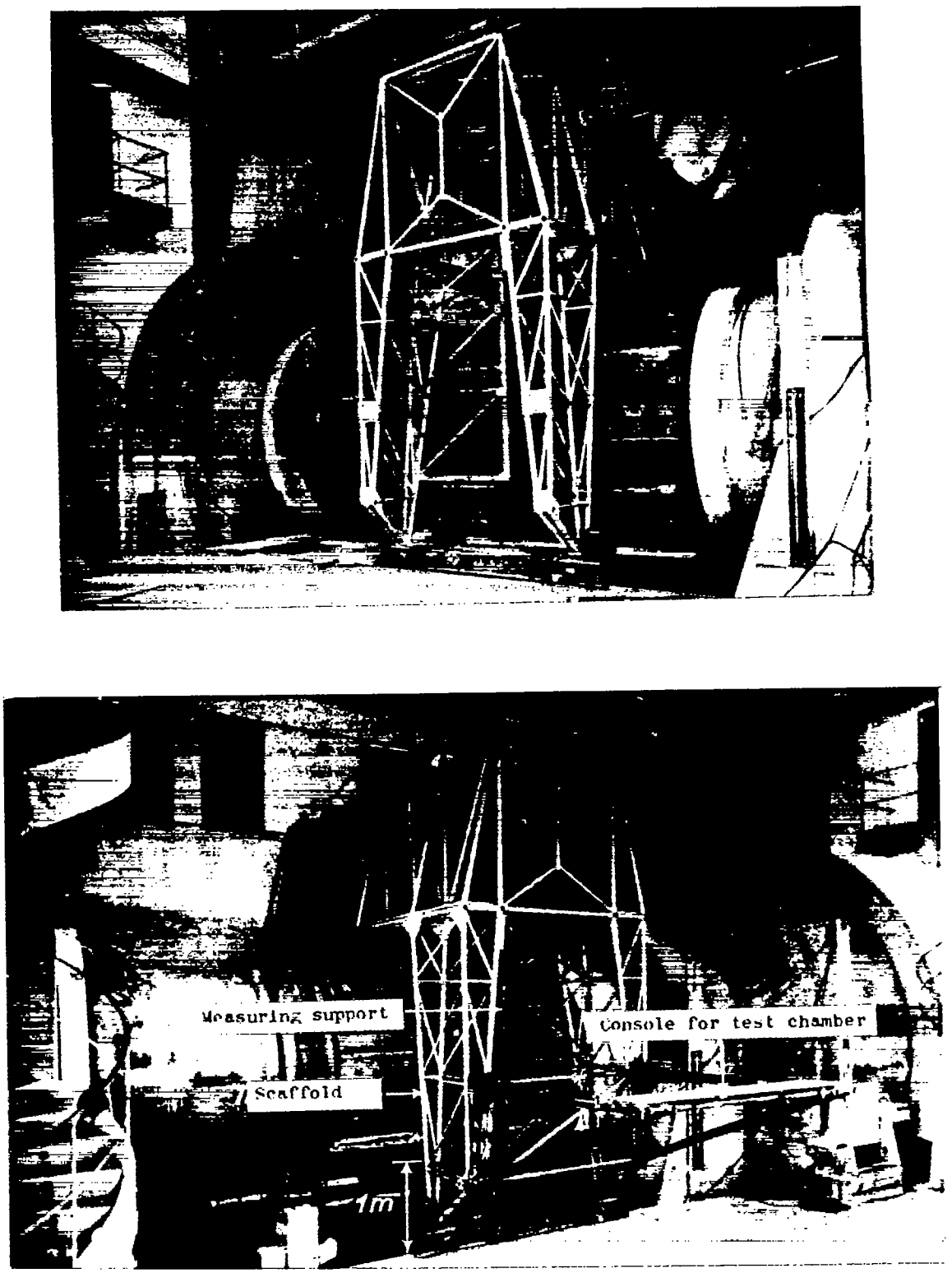

Figure 6.- Traveling scaffold of the interference-schlieren apparatus of the LFA at the test section of the high-speed wind tunnel.

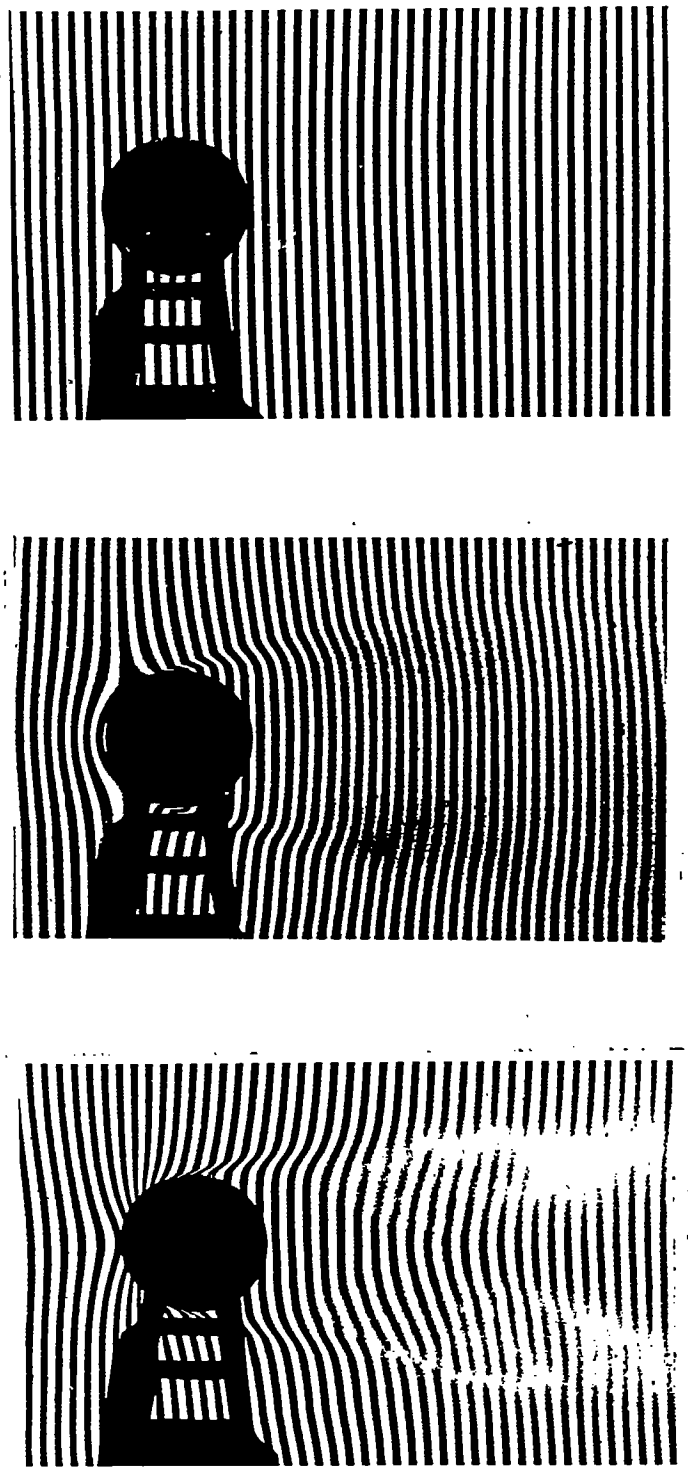

Figure 7.- Density field of circular cylinder in air stream.
D = 25 millimeter φ; v = 75 m/s; L = 170 millimeter length.

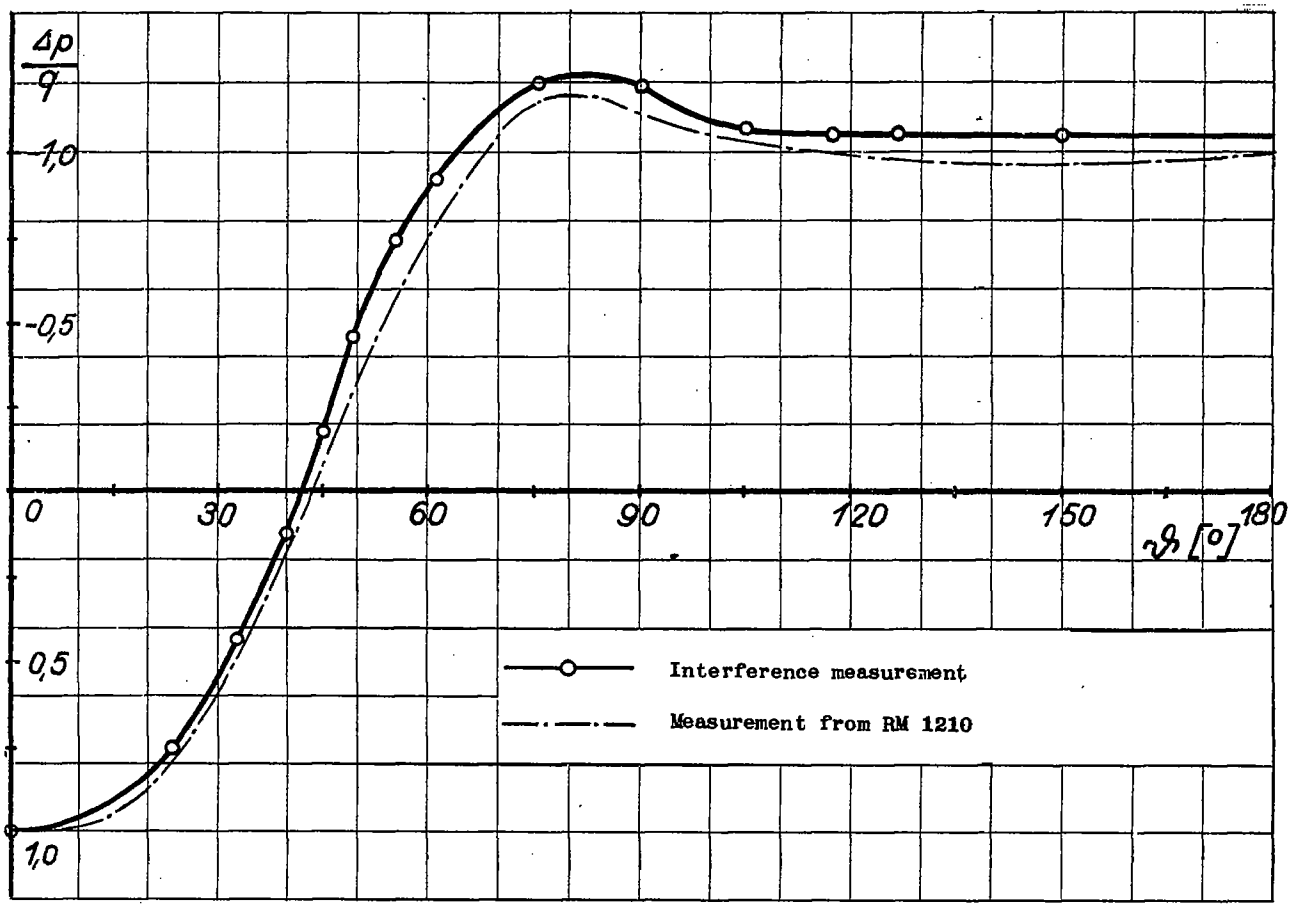

Figure 8.- Pressure distribution on the circular cylinder.

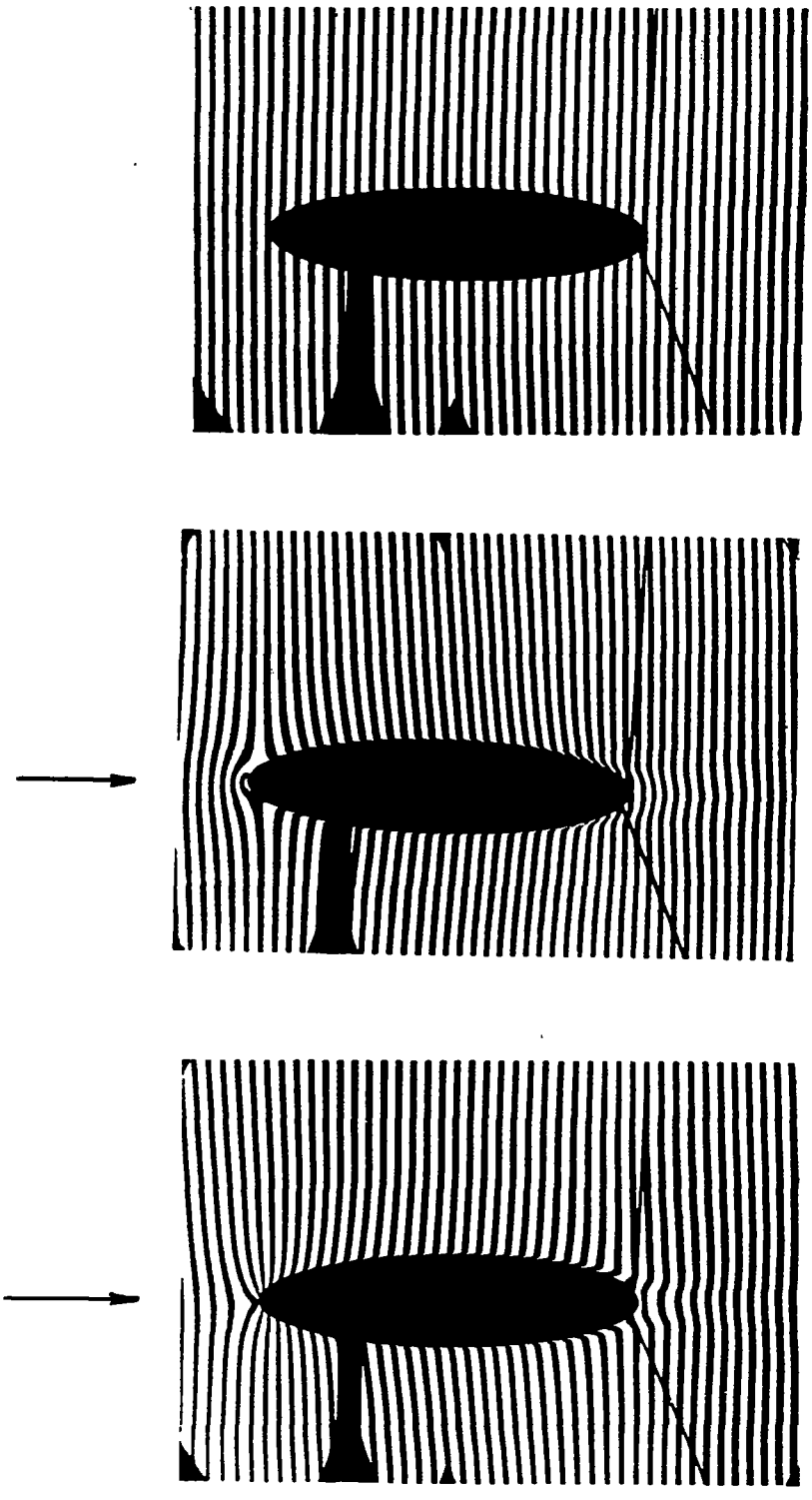

Figure 9.- Density field of the elliptical cylinder for zero angle of attack. 2a = 80 millimeter; $\frac{b}{a} = \frac{1}{4}$; L = 170 millimeter; v = 75 m/s.

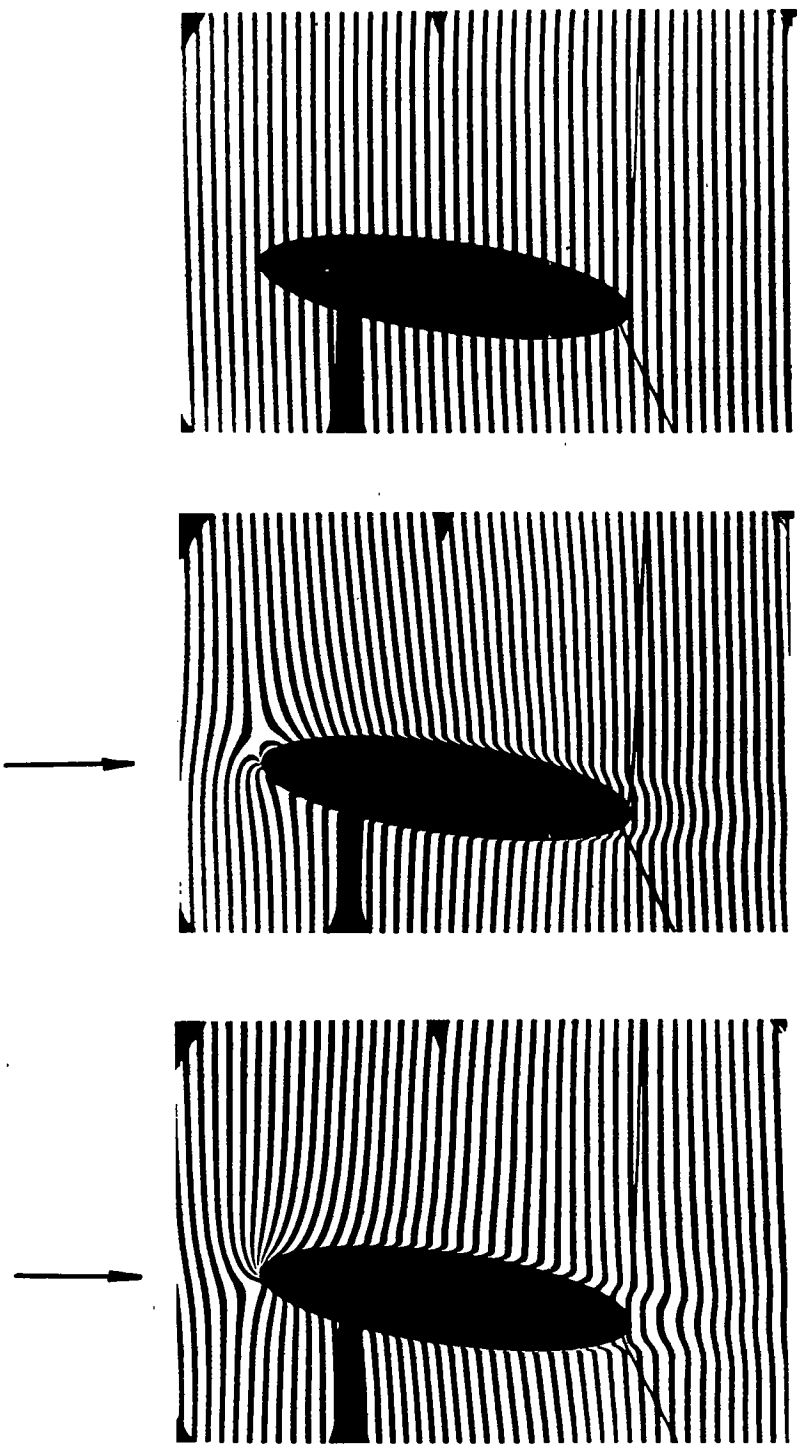

Figure 10.- Density field of the elliptical cylinder for $\alpha = 8^{\circ}$. 2a = 80 millimeter; $\frac{b}{a} = \frac{1}{4}$; L = 170 millimeter; v = 75 m/s.

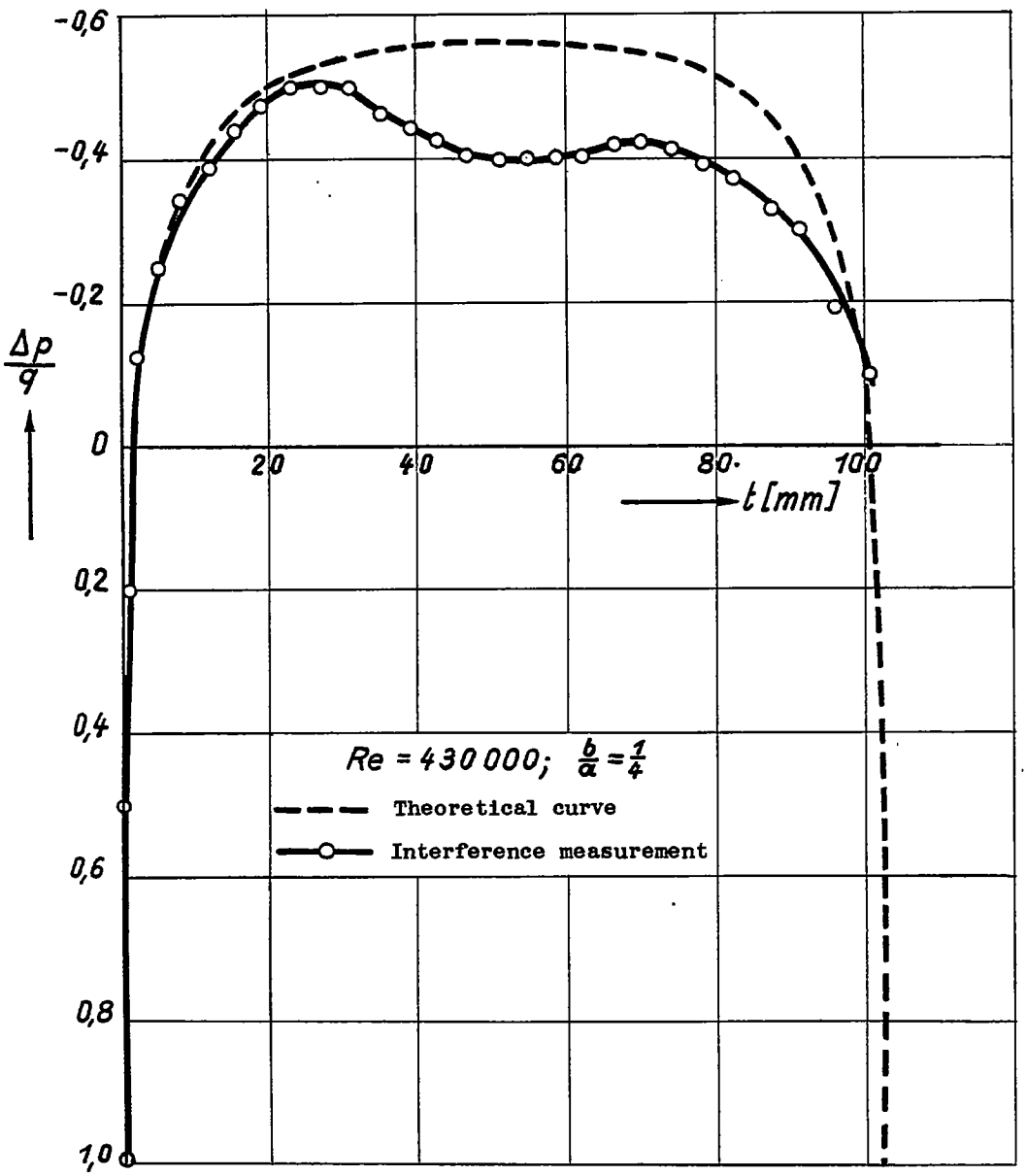

Figure 11.- Pressure distribution on the elliptical cylinder $\alpha = 0^{\circ}$.

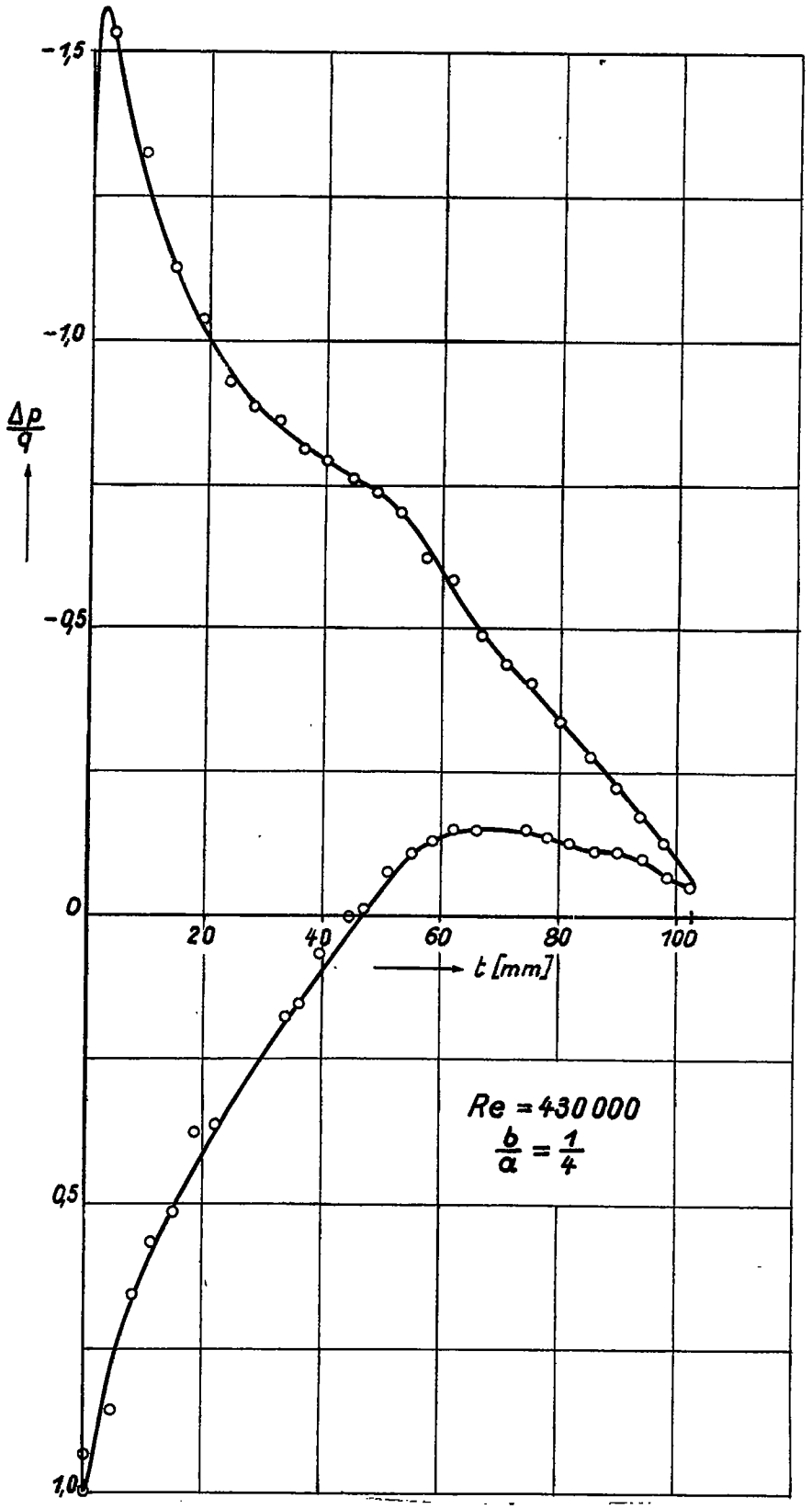

Figure 12.- Pressure distribution on the elliptical cylinder $\alpha = 8^{\circ}$.

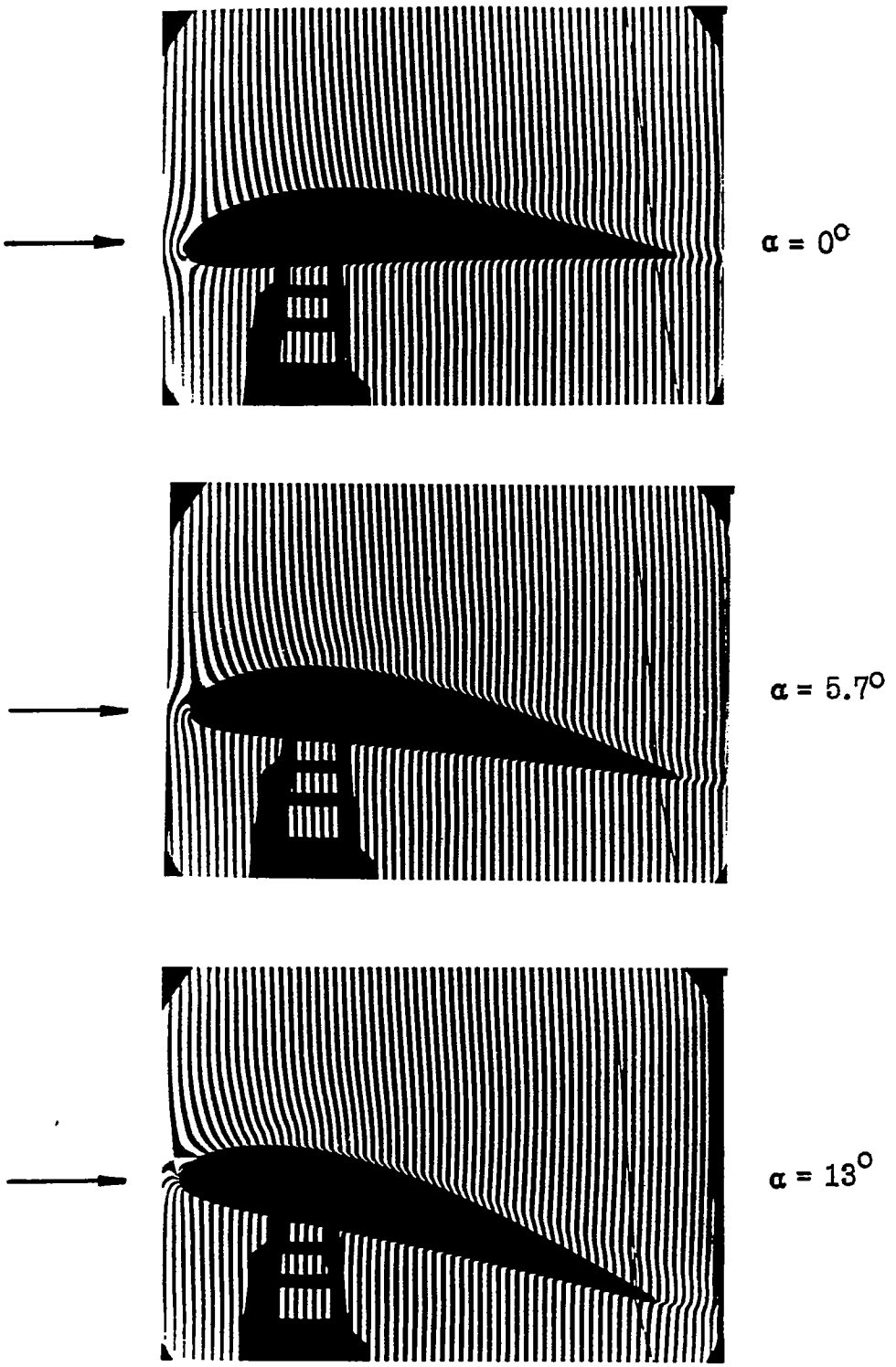

Figure 13.- Density field of the profile Gö 387. t = 120 millimeter wing chord; L = 170 millimeter span; v = 75 m/s.

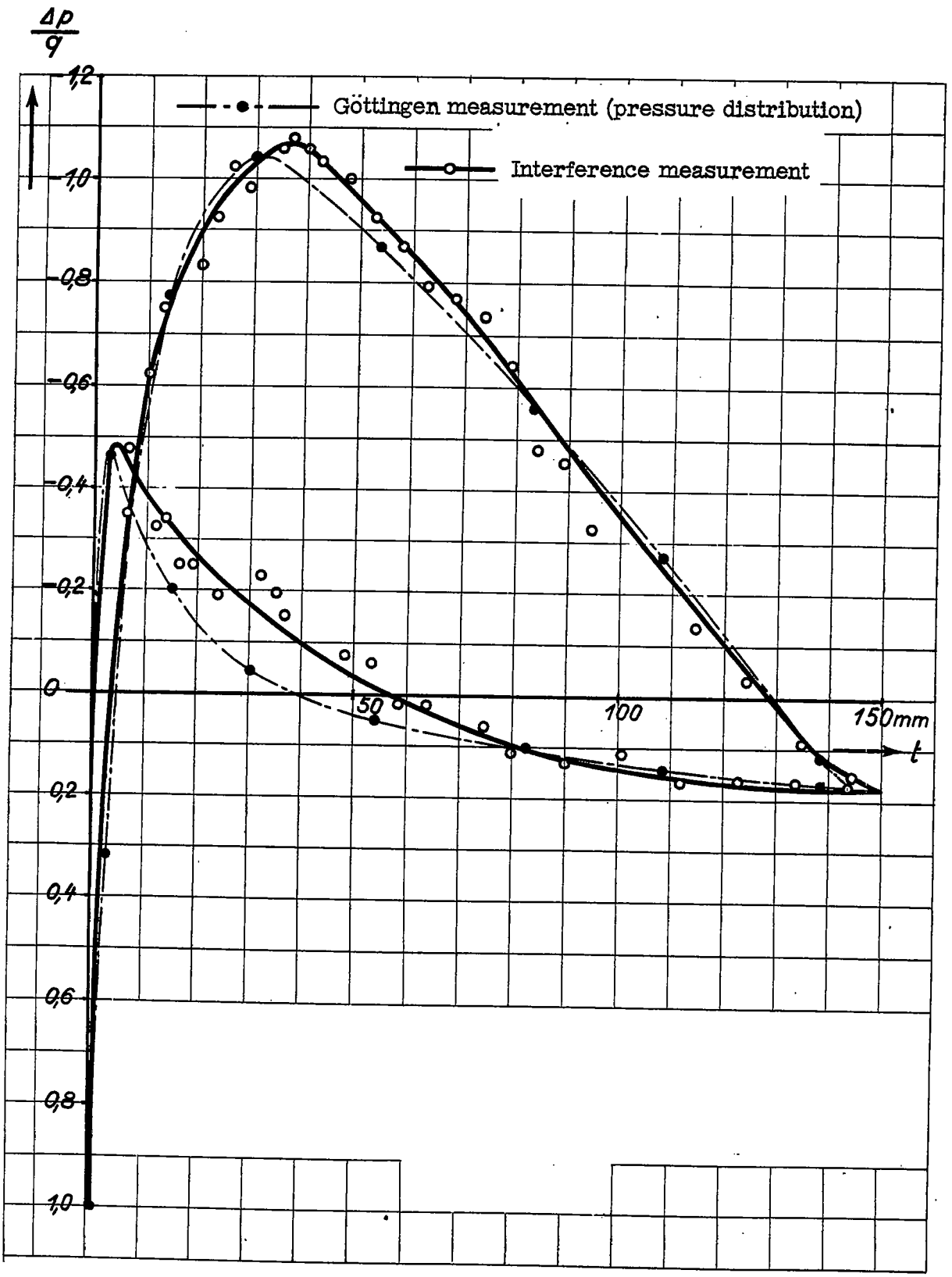

Figure 14.- Pressure distribution on the profile Gö 387; $\alpha = 0^{o}$.

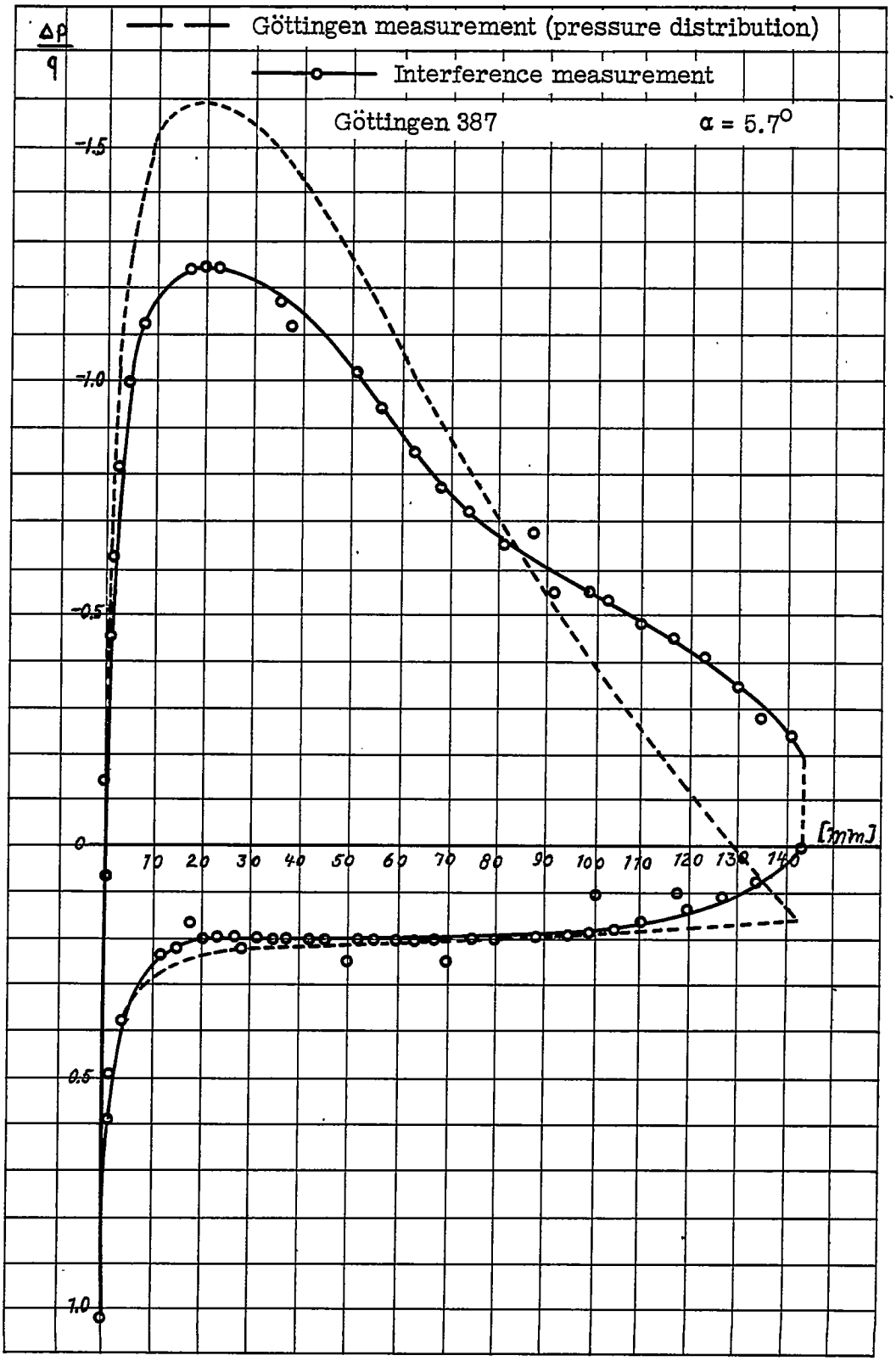

Figure 15.- Effect of the attachment of the profile support on the pressure distribution.

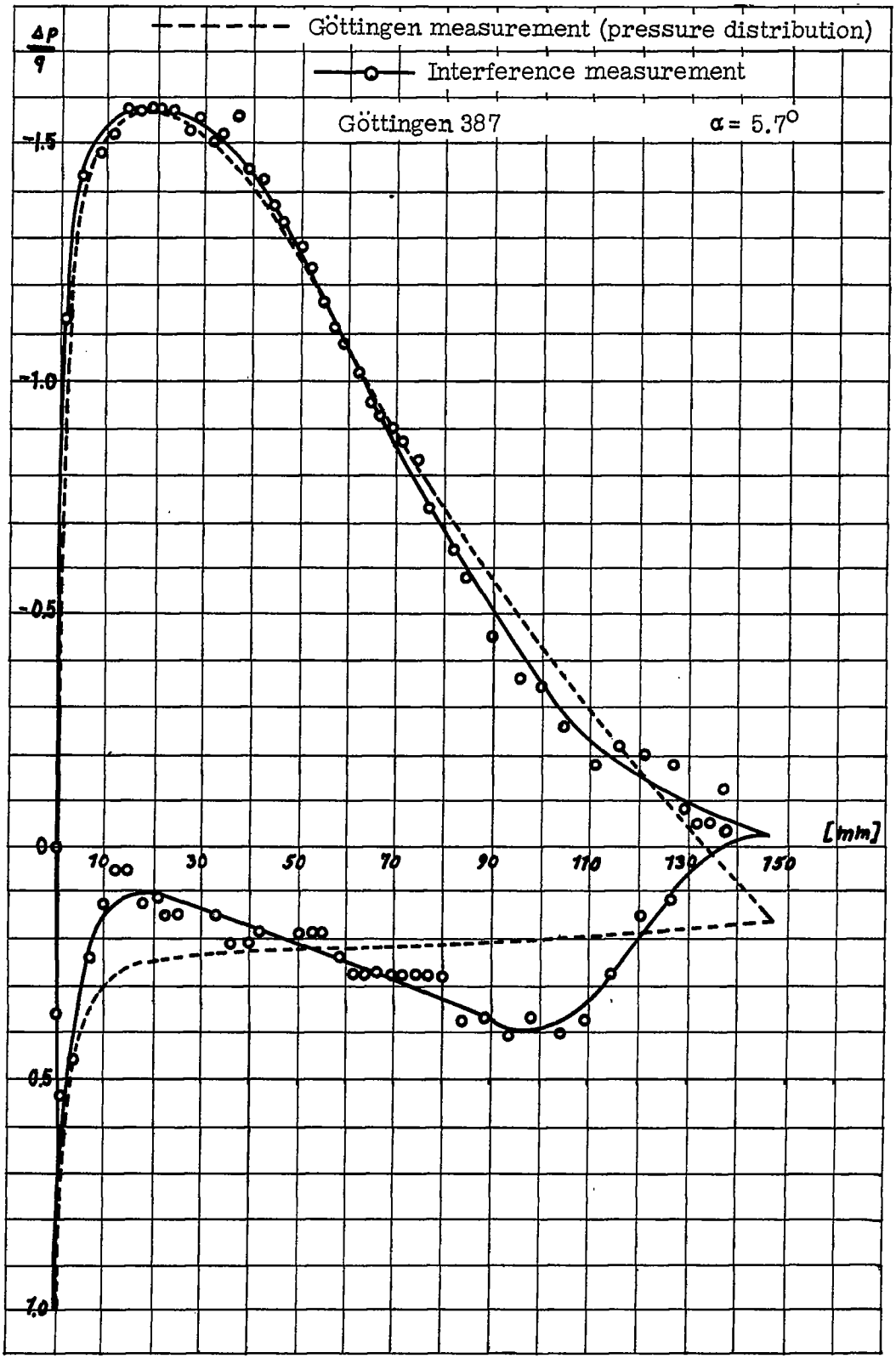

Figure 16.- Effect of the attachment of the profile support on the pressure distribution.

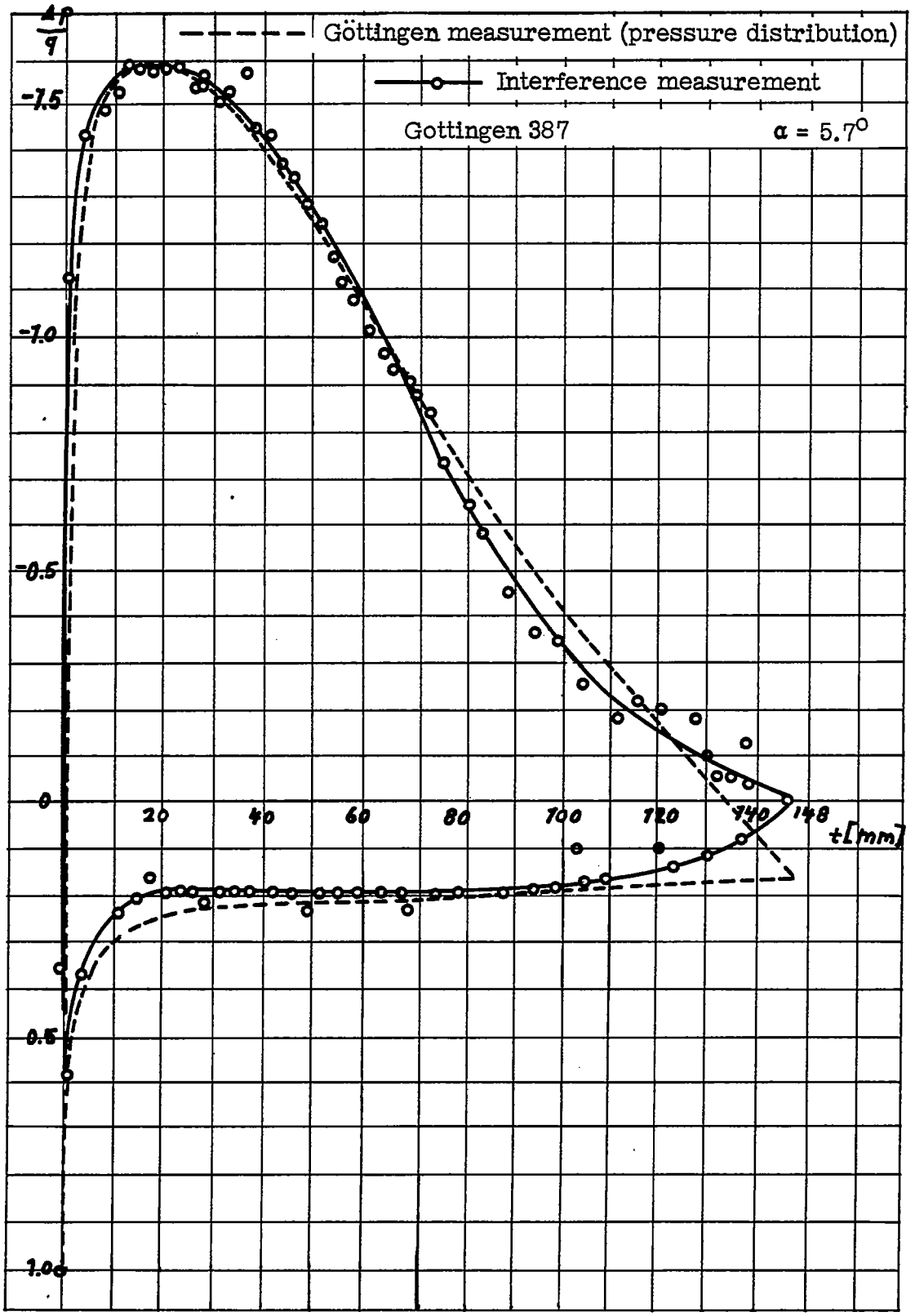

Figure 17.- Effect of the attachment of the profile support on the pressure distribution.

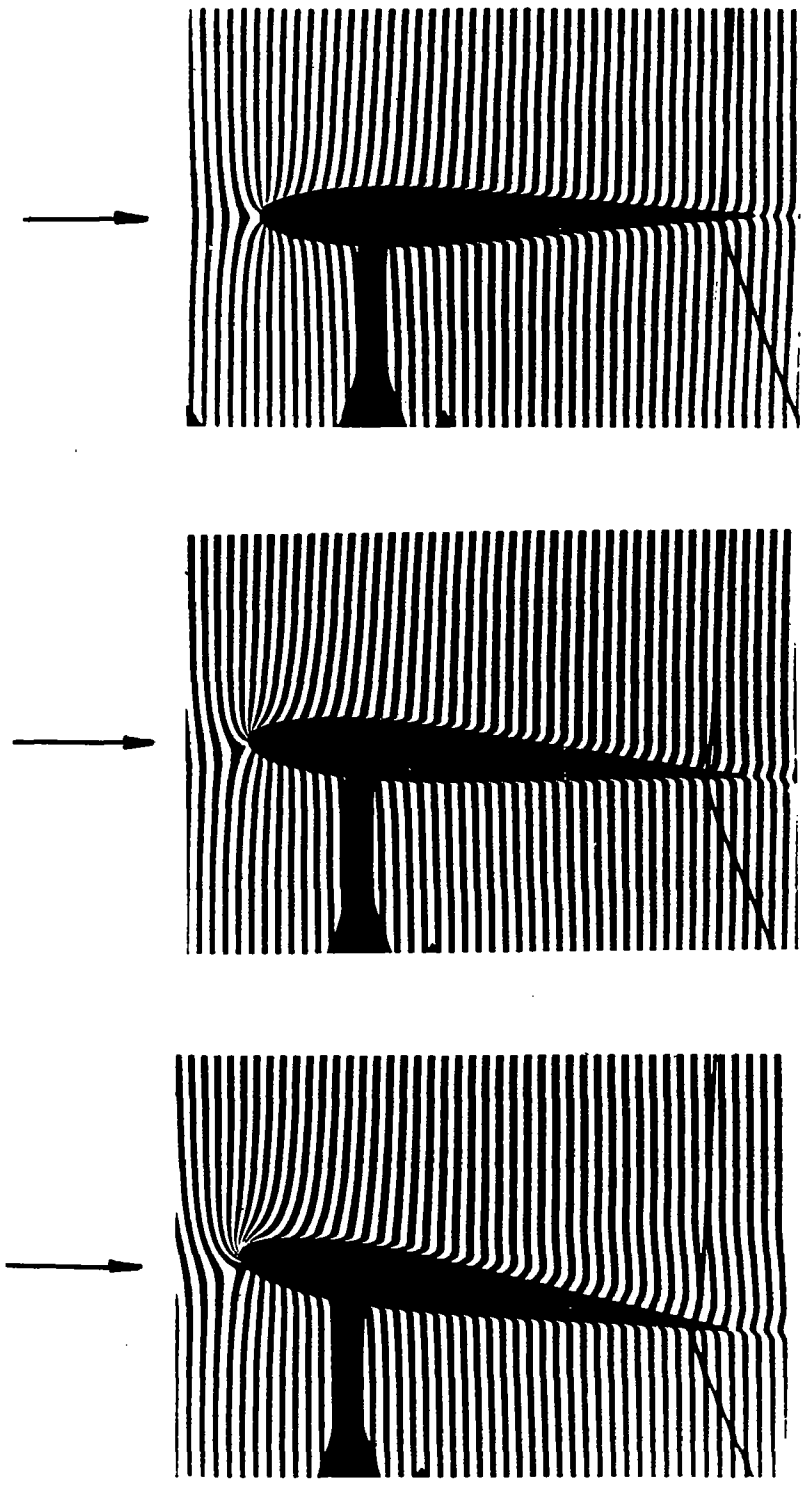

Figure 18.- Density field of the symmetrical Joukowsky profile.
t = 90 millimeter wing chord; L = 170 millimeter span; v = 75 m/s.

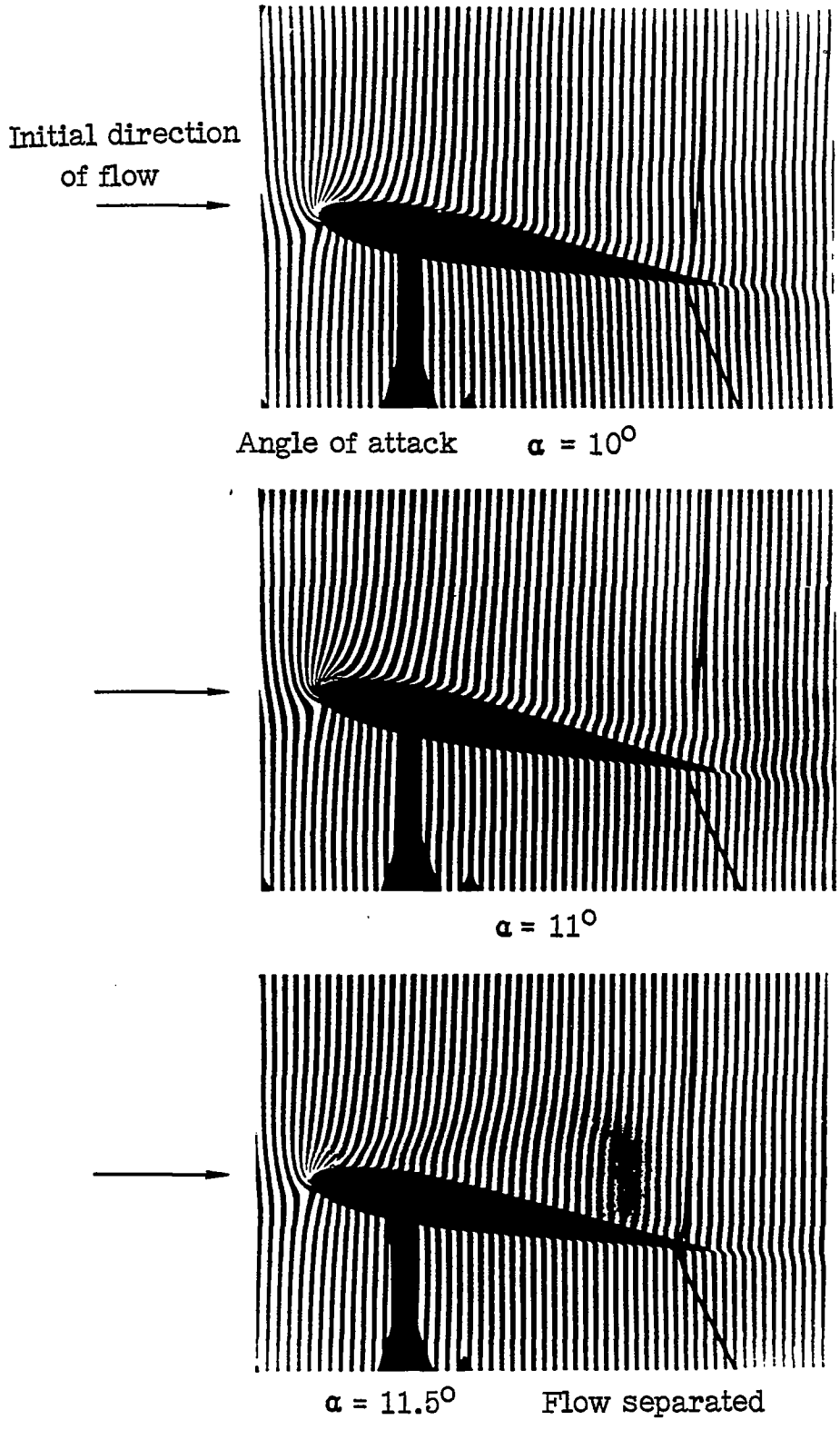

Figure 19.- Density field of the symmetrical Joukowsky profile.
t = 90 millimeter wing chord; L = 170 millimeter span; v = 75 m/s.

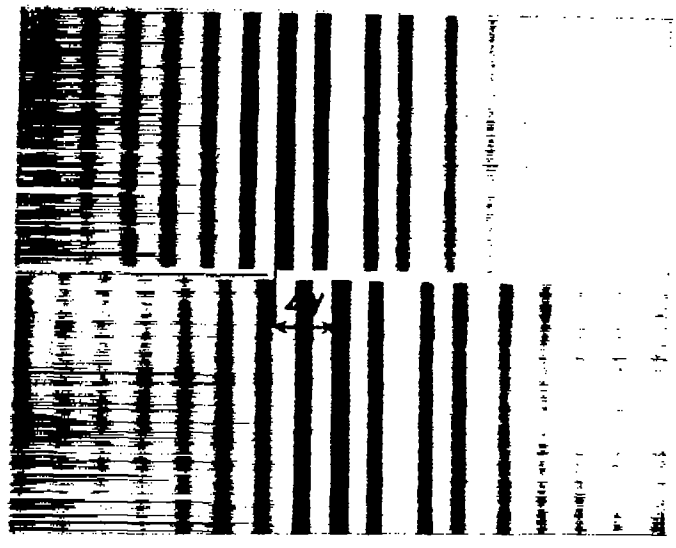

Figure 20.- Null interference with unfiltered mercury light.

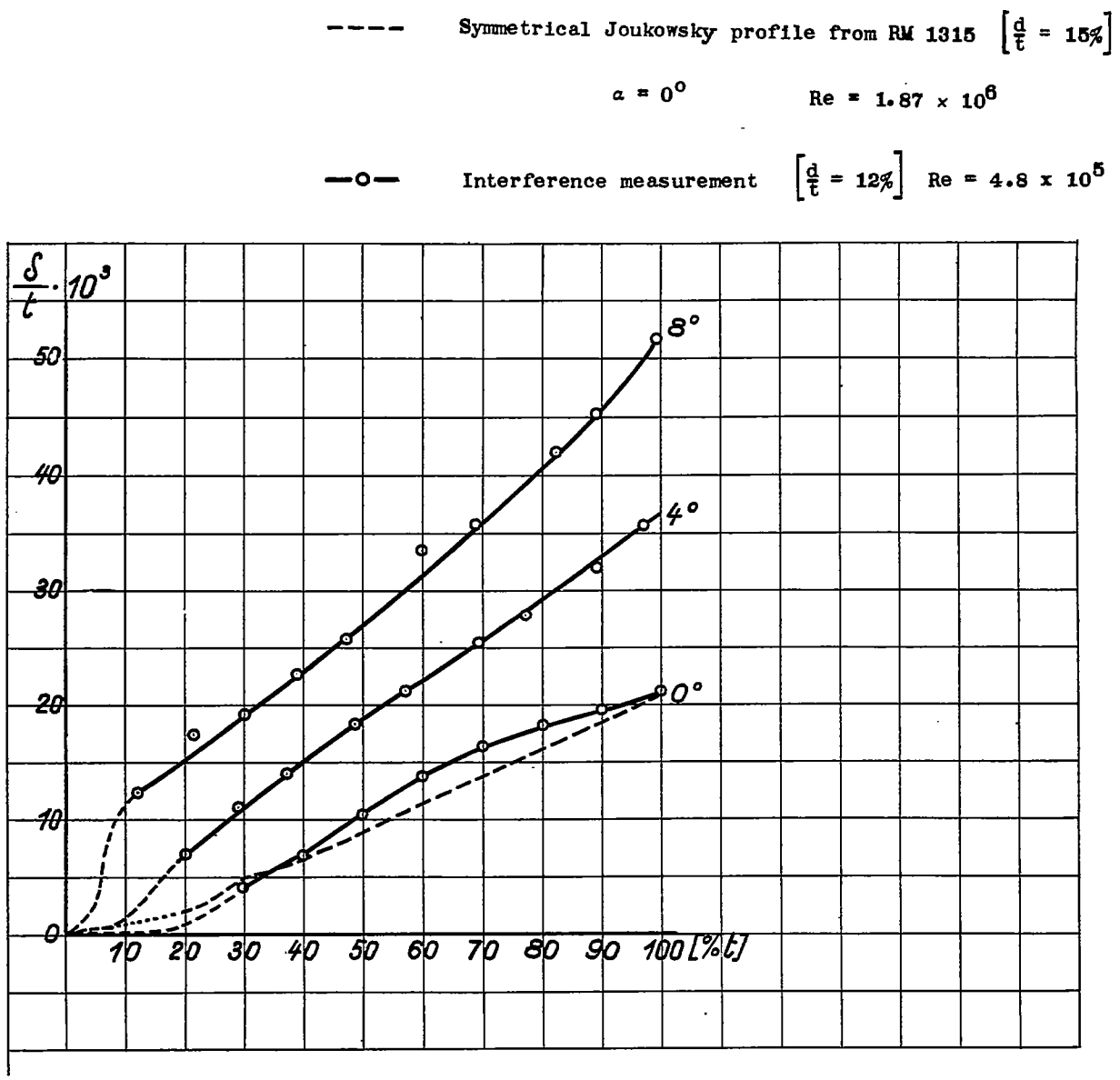

Figure 21.- Boundary-layer thickness on the Joukowsky profile for $\alpha = 0^{\circ}; 4^{\circ}; 8^{\circ}$.

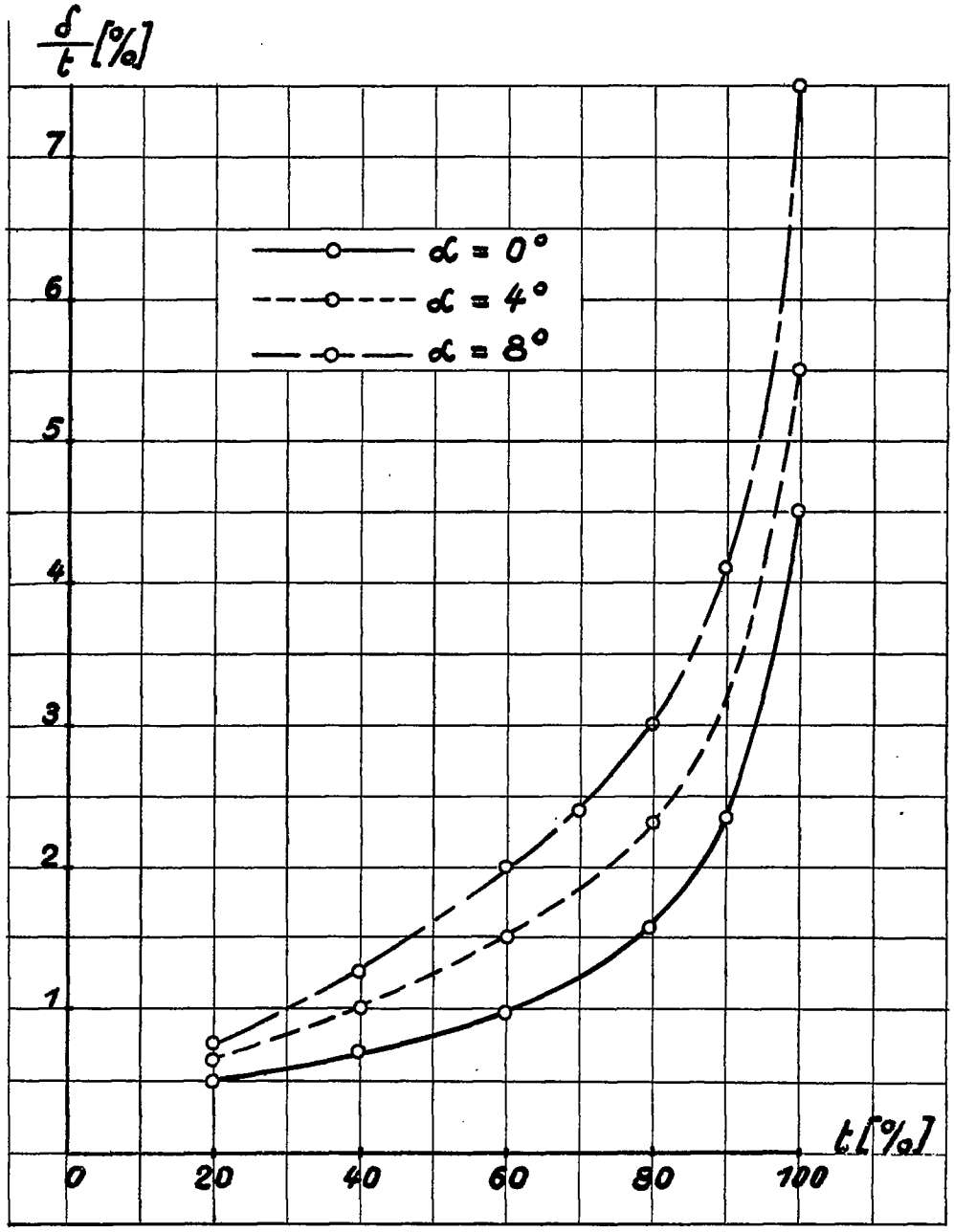

Figure 22.- Boundary layer thickness on the elliptical cylinder.
v = 75 m/s; $\frac{b}{a} = \frac{1}{4}$; 2a = 80 millimeter.

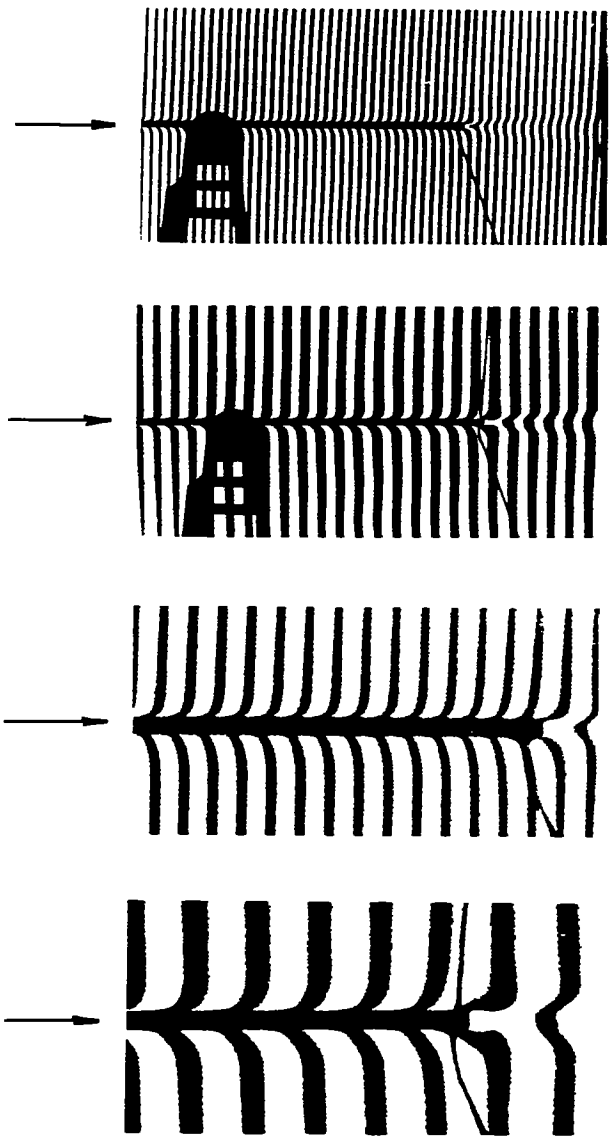

Figure 23.- Boundary layer formation on a flat plate.

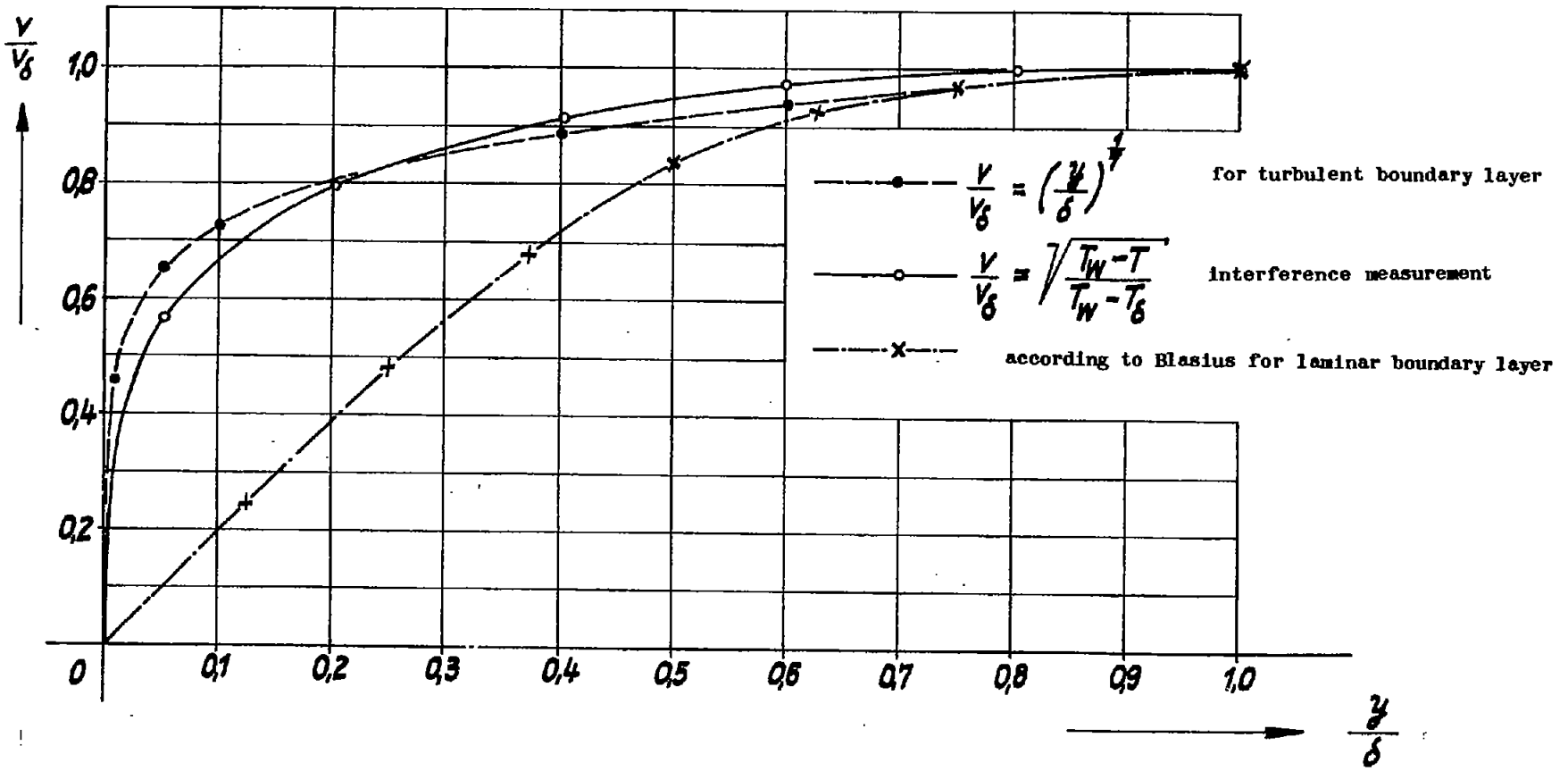

Figure 24.- Velocity distribution in the boundary layer. Flat plate. v = 75 m/s; t = 0.14 m.

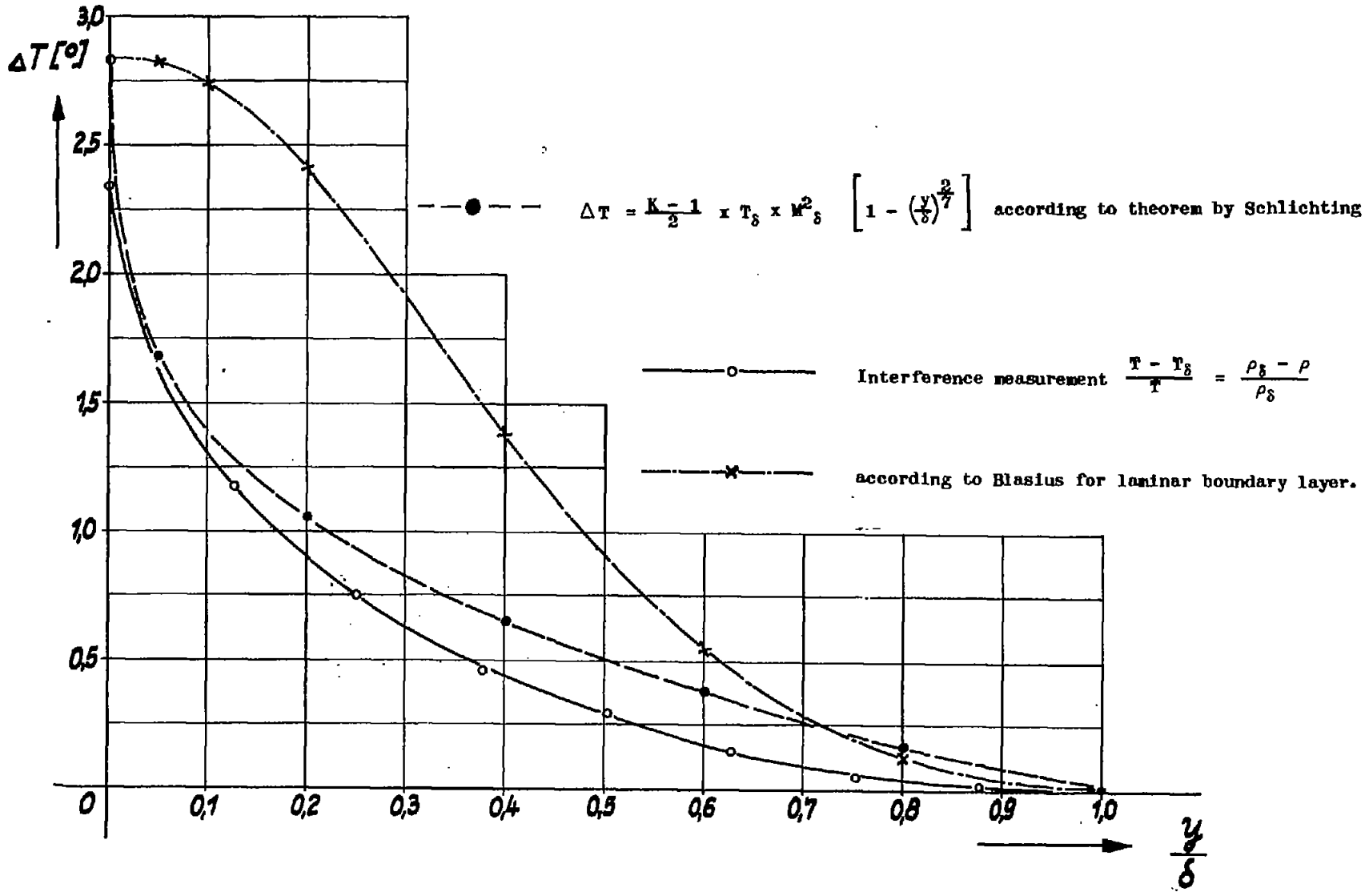

Figure 25.- Temperature distribution in the boundary layer. Flat plate. v = 75 m/s; T_δ = 290°; t = 0.14 m.

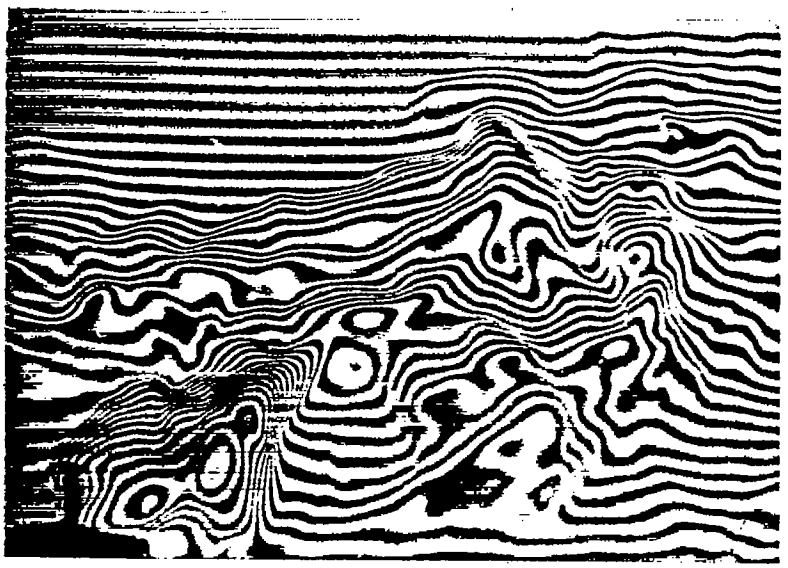

Figure 26.- Unstationary density field around a burning flame. Time of exposure, 1/1000 s.

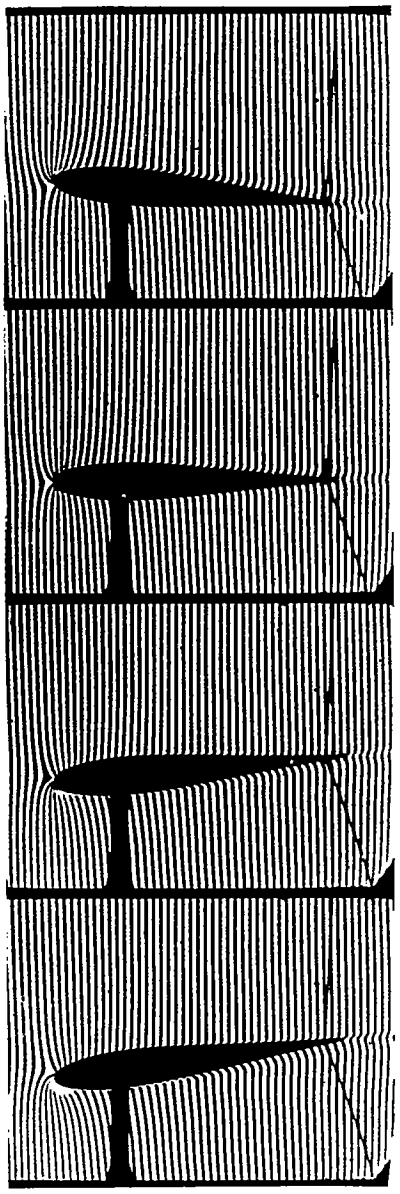

(a) Original photograph.

Figure 27.- Oscillating Joukowsky wing in air stream. n = 40 cycles per second; v = 75 m/s.

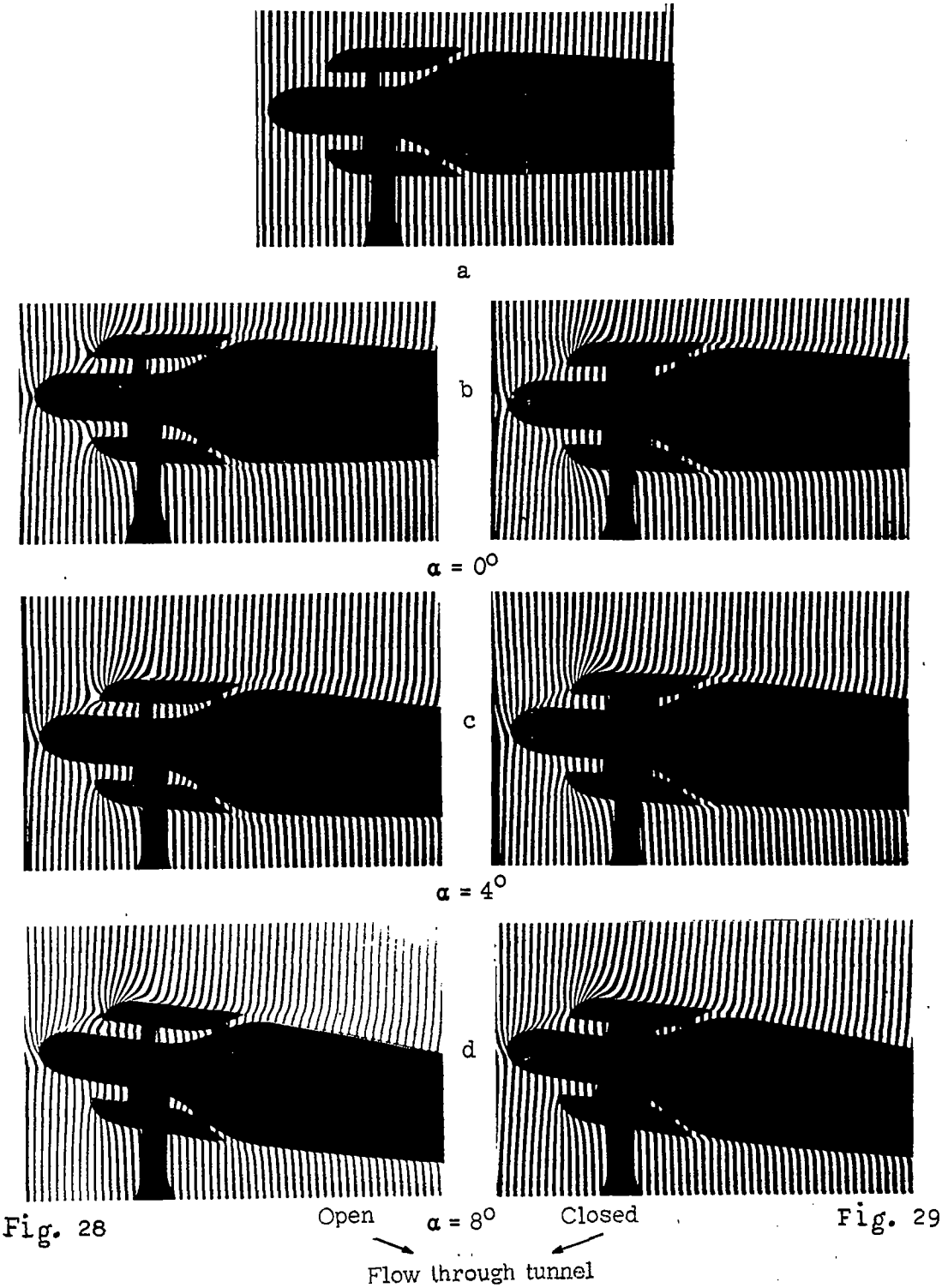

Fig. 28 Fig. 29

Figure 28.- Interference fringe field of flow for a NACA radiator cowl with extended hub, with open air passage; v = 75 m/s.

Figure 29.- Interference fringe field of flow for a NACA radiator cowl with extended hub, with closed air passage; v = 75 m/s.

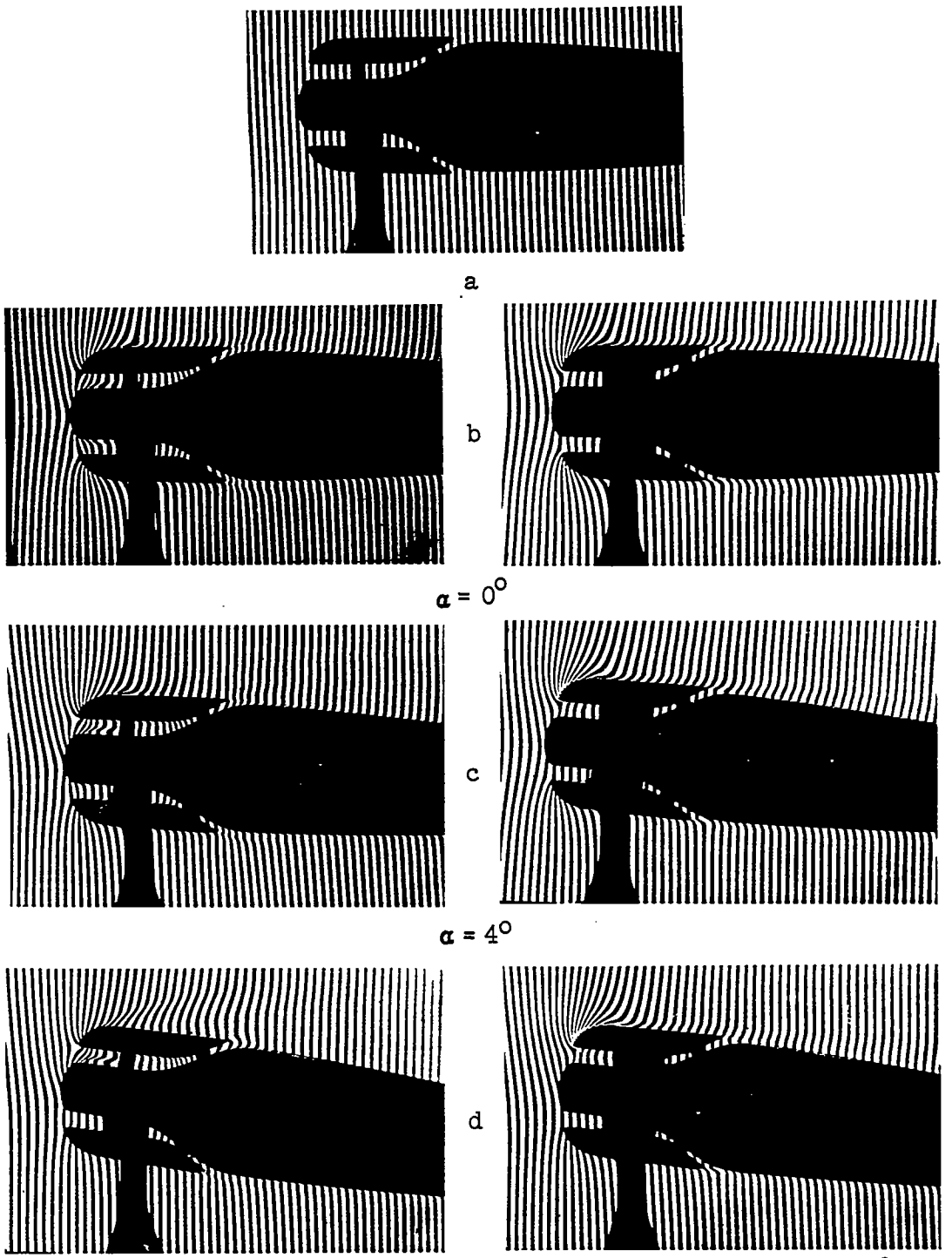

Fig. 30 Fig. 31

Figure 30.- Interference fringe field of flow for a NACA radiator cowl with short hub, with open air passage; v = 75 m/s.

Figure 31.- Interference fringe field of flow for a NACA radiator cowl with short hub, with closed air passage; v = 75 m/s.

Interference fringe field of flow in a jet-type radiator for extremely large air passage; v = 75 m/s.

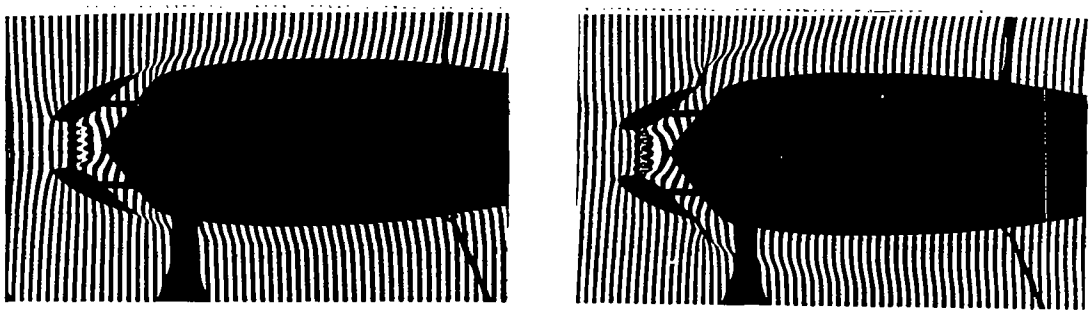

$\alpha = 0^{\circ}$

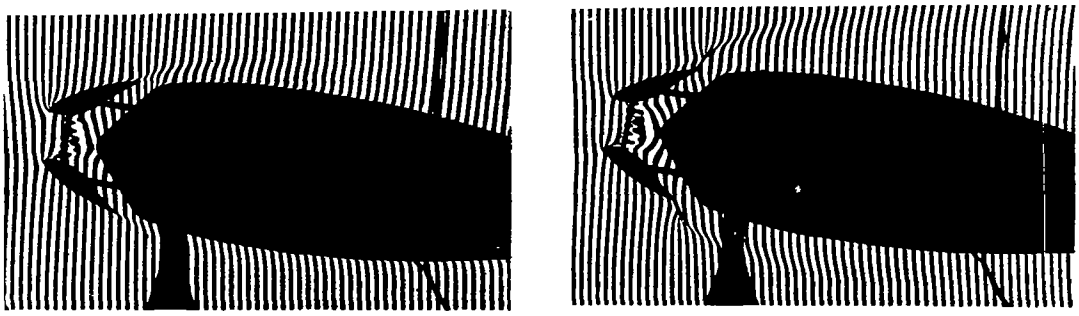

Fig. 32 $\alpha = 8^{\circ}$ Fig. 33

Without ——— With

Extended flap

Figure 32.- Radiator with transmitting drag plate as cooling block, for $\alpha = 0^{\circ}$; $\alpha = 8^{\circ}$; without extended flap.

Figure 33.- Radiator with transmitting drag plate as cooling block, for $\alpha = 0^{\circ}$; $\alpha = 8^{\circ}$; with extended flap.

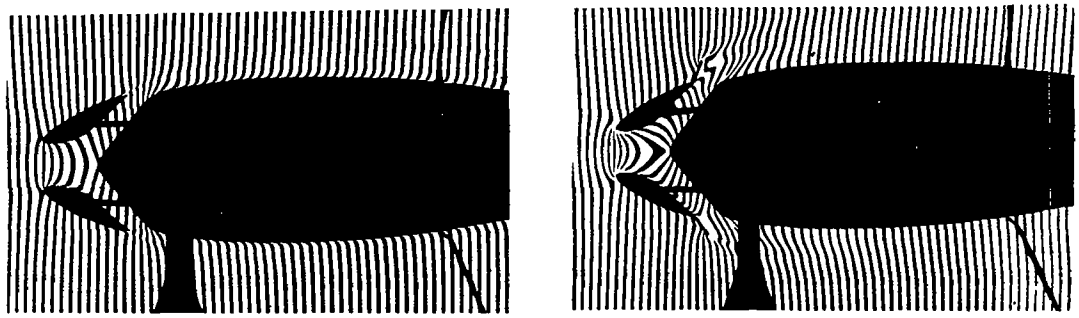

Fig. 34 $\alpha = 0^{\circ}$ Fig. 35

Without ——— With

Extended flap for open air passage.

Figure 34.- Without extended flap, for open air passage, $\alpha = 0^{\circ}$.

Figure 35.- With extended flap, for open air passage, $\alpha = 0^{\circ}$.